INTERNATIONAL JOURNAL FOR NUMERICAL METHODS IN ENGINEERING
Int. J. Numer. Meth. Engng 2016; **108**:535–567
Published online 25 February 2016 in Wiley Online Library (wileyonlinelibrary.com). DOI: 10.1002/nme.5221

Linear unconditional energy-stable splitting schemes for a phase-field model for nematic–isotropic flows with anchoring effects

Francisco Guillén-González[1,*,†], María Ángeles Rodríguez-Bellido[1] and Giordano Tierra[2]

[1]*Departamento de Ecuaciones Diferenciales y Análisis Numérico and IMUS, Universidad de Sevilla, Aptdo. 1160, 41080 Seville, Spain*
[2]*Department of Mathematics, Temple University, 1805 N. Broad Street (Wachman Hall), Philadelphia PA 19122, USA*

SUMMARY

Two-phase flows composed of fluids exhibiting different microscopic structure are an important class of engineering materials. The dynamics of these flows are determined by the coupling among three different length scales: microscopic inside each component, mesoscopic interfacial morphology, and macroscopic hydrodynamics. Moreover, in the case of complex fluids composed by the mixture between isotropic (Newtonian fluid) and nematic (liquid crystal) flows, its interfaces exhibit novel dynamics due to anchoring effects of the liquid crystal molecules on the interface.

Firstly, we have introduced a new differential problem to model nematic–isotropic mixtures, taking into account viscous, mixing, nematic, and anchoring effects and reformulating the corresponding stress tensors in order to derive a dissipative energy law. Then, we provide two new linear unconditionally energy-stable splitting schemes. Moreover, we present several numerical simulations in order to show the efficiency of the proposed numerical schemes and the influence of the different types of anchoring effects in the dynamics of the system. Copyright © 2016 John Wiley & Sons, Ltd.

Received 26 August 2015; Revised 23 December 2015; Accepted 19 January 2016

KEY WORDS: liquid crystal; phase field; finite elements; multiphase flows; energy stability; anchoring effects

1. INTRODUCTION

The study of interfacial dynamics between two different components has become the key role to understand the behavior of many interesting systems, with applications in science, engineering, and industry. For instance, the dynamics of an interface that separates two (or more) materials arise naturally in hydrodynamics applications or in solidification processes. We can find a big amount of applications related to phase separation, like liquid crystals, vesicle membranes deformation, image processing, and tumor growth.

An efficient and physically relevant approach for solving interface problems is due to the diffuse interface theory, which is based on describing the interfaces by layers of small thickness and whose structure is determined through a non-local mixing energy that captures the balance of molecular forces, where this energy represents the competition for mixing and de-mixing processes. These ideas were already considered by van der Waals [1] and can be considered the foundation of the

*Correspondence to: Francisco Guillén-González, Departamento de Ecuaciones Diferenciales y Análisis Numérico and IMUS, Universidad de Sevilla, Aptdo. 1160, 41080 Seville, Spain.
†E-mail: guillen@us.es

phase-field theory for phase transition and critical phenomena. In the diffuse interface theory, the surface motion can be derived as the dissipation of a phase field's free energy functional $E_\varepsilon(\phi)$,

$$\phi_t = \frac{\delta E_\varepsilon(\phi)}{\delta \phi},$$

where ϕ denotes the so-called phase-field function that is used to localize the components inside the system, assuming that ϕ takes different stable values for each phase (for instance, $\phi = 1$ in one phase and $\phi = -1$ in the other one). The key point is to consider that in the interfacial regions, the function varies smoothly, making feasible to define the function ϕ in the whole domain. This fact provides many interesting properties like easiness of coupling with physical variables, indifference to morphological singularities in the interface, or the possibility of considering a global space discretization.

In this work, we are interested in the diffuse interface approach to represent mixtures composed of isotropic fluids and nematic liquid crystals. Liquid crystals can be viewed as a state of matter that exhibits properties between liquids and solids. Macroscopically, liquid crystals behave like liquids, but in the microscopic scale, their molecules have an orientational property due to elasticity effects (i.e., liquid crystals can be viewed as anisotropic liquids). There are several types of liquid crystals and can be classified as thermotropic and lyotropic, whose change of state depends on varying the temperature or the concentration, respectively.

Examples of liquid crystals can be widely found in nature and technological applications. For instance, most contemporary electronic devices use liquid crystals for their displays, and lyotropic liquid-crystalline phases can be found in living systems, forming proteins and cell membranes. There are two main groups of thermotropic liquid crystals (Figure 1): nematic and smectic. On one hand, nematic phases are formed by rod-shaped molecules with no positional order, although their molecules are able to self-align in order to have a long-range directional order parallel with respect to their long axes. On the other hand, smectic phases (which are found at lower temperatures than the nematic ones) are positionally ordered along one direction forming well-defined layers that can slide over one another, acting like liquids within each layer. In particular, in smectic-A phases, the molecules are oriented along the normal vector of the layers, while in smectic-C phases, they are tilted away from the normal vector of the layer. For further information on the physics and properties of the different liquid crystals, we refer the reader to [2].

In order to understand the behavior of the models representing complex fluids composed of mixtures of isotropic fluids and nematic liquid crystals, it is needed to combine ideas from fluid dynamics, phase-field models, mixtures of fluids, and nematic liquid crystals. The amount of literature related to these topics is extremely huge, and it is impossible to make a fair description of all the results or approaches that can be considered. For that reason, we just mention here some

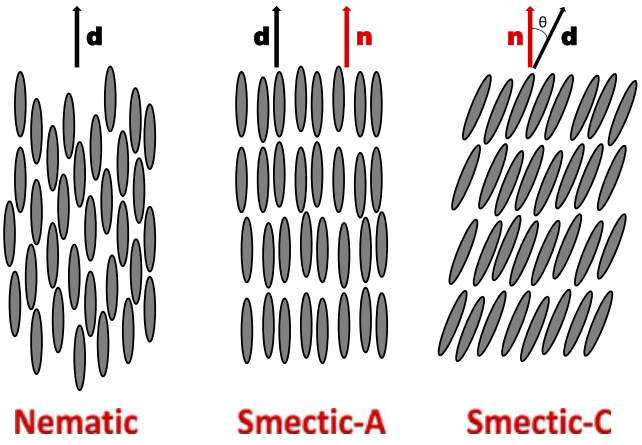

Figure 1. Different phases of thermotropic liquid crystals.

DOI: 10.1002/nme

overviews on the state of the art on the study of phase-field models [3], mixtures of fluids [4], and mathematical study (theoretically and numerically) of liquid crystals [5, 6].

In recent times, the interest of studying systems representing the interaction between Newtonian and nematic fluids has grown considerably in both the mathematics and the physics communities. There have been different approaches to simulate this type of models. The authors of [7] study the kinetics of the nematic–isotropic transition in a two-dimensional liquid crystal by using a lattice Boltzmann scheme that couples the tensor order parameter and the flow, finding that the time dependences of the correlation function, energy density, and number of topological defects arise from dynamic scaling laws. In [8], the authors considered another ideas, using the Landau–de Gennes free energy to calculate the interaction between long cylindrical colloids and the nematic–isotropic interface. In [9], it is presented an approach to compute the shape and internal structure of two-dimensional nematic drops. Using these techniques, they are able to calculate the director field for a given domain shape. In [10], the authors explore experimentally the structure of nuclei and topological defects in the phase transition between the nematic and isotropic phases in lyotropic chromonic liquid crystals, demonstrating the important role played by the surface anisotropy in morphogenesis of phase transitions in liquid crystals. Another coupling that has recently attracted attention in the community is the one between isotropic fluids with cholesteric liquid crystals. It is known that this interface can display a range of unusual properties, such as a layer of topological defects close to an undulated interface, but the dynamics and composition of this interface remains still poorly understood. We refer the reader to [11] for a calculation of the structure and surface tension of the cholesteric–isotropic interface.

From the mathematical point of view, the first attempt to represent this coupling by using a phase-field approach was presented in [12, 13]. In these works, the authors presented an energy-based approach that makes it possible to incorporate complex rheology easily, and they also present some numerical simulations. The authors in [14] explore the coupling among bulk liquid crystal orientation, surface anchoring, and the flow field, showing that the anchoring energy plays a fundamental role in the interfacial dynamics of nematic liquids. More recently, in [15], the authors present an energy-based phase-field model for the coupling of a nematic liquid crystal phase in a viscous fluid phase, presenting coupled numerical schemes with several simulations. This work was extended in [16], where the authors presented a splitting numerical scheme for this model. Energy laws are obtained there for the continuous problem and discrete scheme, designing linear unconditionally stable numerical schemes. However, in this work, the anchoring effects were not taken into account in the numerical analysis, and the interpolation function that they consider to localize the nematic region cannot be arbitrary.

In this work, we study a modification of the model presented in [16] where we take into account the anchoring effects and an arbitrary interpolation function can be considered to localize the nematic region (in practice, we consider a fifth-order polynomial). We derive new linear splitting schemes for nematic–isotropic mixtures, taking into account viscous, mixing, nematic, and anchoring effects, which allows us to split the computation of the three pairs of unknowns $(\boldsymbol{v}, p)$ (velocity–pressure), (c, μ) (phase field–chemical potential), and $(\boldsymbol{d}, \boldsymbol{w})$ (director vector–equilibrium) in three different steps. The derivation of these new decoupled schemes are inspired by the ideas previously presented in [17–19]. Moreover, we have proven that these formulations are unconditionally energy stable (independently of the size of space and time meshes considered). Finally, we present several numerical simulations to illustrate the correct behavior of the proposed numerical schemes and to show the dependence of the dynamics on the different types of anchoring effects that can be considered.

This work is organized as follows. In Section 2, we present the model that we are considering jointly with the main ideas for deriving it and a reformulation of the problem adding some auxiliary variables that will allows us to consider C^0 finite elements to discretize the system in space. Section 3 is devoted to design the new numerical schemes and to show their unconditional energy stability, detailing the splitting ideas and how to discretize the potentials in a linear and energy-stable way. In Section 4, we present several numerical experiments in order to show the efficiency of the proposed numerical schemes and the influence of the anchoring effects on the dynamics of the system. Finally, in Section 5, we state the conclusions of our work.

DOI: 10.1002/nme

2. THE MODEL

In this section, we describe the multicomponent complex fluid mixture subject of our study, consisting of two phases: a nematic liquid crystal and a Newtonian fluid.

The model considered is based on the one presented in Reference [12], where the authors proposed a way of deriving models for mixtures of complex fluids. The idea is based on using a phase-field function to localize inside the domain the region where each component is contained. The total energy of the system is represented as the sum of the internal energies of each one of the components plus the mixture energy associated to the phase-field system [20]. Then, the key point is to consider a phenomenological derivation, giving first a total free energy (that depends on an average of the considered effects: kinetic, interfacial, nematic, and anchoring) and arriving at a thermodynamically consistent PDE system with respect to this free energy. These ideas have been successfully extended to model different complex fluid systems like mixtures, liquid crystals, biofilms, vesicles membranes, or ion channels [21–28].

Let us present in detail the derivation of a mixture of a nematic liquid crystal and a Newtonian fluid, where for the sake of simplicity we assume that both fluids have the same constant density $\rho_{Nem} = \rho_{Iso} = 1$. We consider a bounded domain $\Omega \subset \boldsymbol{R}^{\boldsymbol{M}}$, $(M = 2, 3)$, whose boundary will be represented by Γ (i.e., $\Gamma := \partial\Omega$), and we introduce a phase-field function $c(\boldsymbol{x}, t)$ that will be used to localize the components along the domain Ω, such that

$$c(\boldsymbol{x}, t) = \begin{cases} -1 & \text{Newtonian fluid}, \\ 1 & \text{nematic liquid crystal}. \end{cases}$$

We define the total energy of the system as the addition of the energies related to each component plus the energy associated to the mixture in the interface between both phases:

$$E_{tot}(\boldsymbol{u}, c, \boldsymbol{d}) = E_{kin}(\boldsymbol{u}) + \lambda_{mix} E_{mix}(c) + \lambda_{nem} E_{nem}(\boldsymbol{d}, c) + \lambda_{anch}\, E_{anch}(\boldsymbol{d}, c), \tag{2.1}$$

where $E_{kin}(\boldsymbol{u})$ denotes the kinetic energy of the system, $E_{mix}(c)$ denotes the mixing energy associated to the mixture process, $E_{nem}(\boldsymbol{d}, c)$ denotes the elastic energy due to the nematic liquid crystal (that also contains a penalization part related to the unitary constraint of the director vector), and $E_{anch}(\boldsymbol{d}, c)$ denotes the anchoring energy that represents the influence of the interfacial effects on the orientation of the nematic liquid crystal molecules in the interface between both components. Moreover, parameters λ_{mix}, λ_{nem}, and λ_{anch} are introduced to balance the effect of each energy in the system. In particular, the energy terms reads

$$\begin{aligned} E_{kin}(\boldsymbol{u}) &= \frac{1}{2}\int_{\Omega} |\boldsymbol{u}|^2 d\boldsymbol{x}, \\ E_{mix}(c) &= \int_{\Omega} \left(\frac{1}{2}|\nabla c|^2 + F(c)\right) d\boldsymbol{x}, \\ E_{nem}(\boldsymbol{d}, c) &= \int_{\Omega} I(c) \left(\frac{1}{2}|\nabla \boldsymbol{d}|^2 + G(\boldsymbol{d})\right) d\boldsymbol{x}, \end{aligned}$$

and the anchoring energy will take different forms depending on the anchoring effect considered,

$$E_{anch}(\boldsymbol{d}, c) = \begin{cases} 0 & \text{no anchoring}, \\ \dfrac{1}{2}\displaystyle\int_{\Omega} \left(|\boldsymbol{d} \cdot \nabla c|^2\right) d\boldsymbol{x} & \text{parallel anchoring}, \\ \dfrac{1}{2}\displaystyle\int_{\Omega} \left(|\boldsymbol{d}|^2 |\nabla c|^2 - |\boldsymbol{d} \cdot \nabla c|^2\right) d\boldsymbol{x} & \text{homeotropic anchoring}. \end{cases}$$

For the functionals $F(c)$ and $G(\boldsymbol{d})$, we assume the following double-well potentials, which, in both cases, have their minimums (and consequently their equilibrium states) at ± 1:

DOI: 10.1002/nme

$$F(c) = \frac{1}{4\varepsilon^2}(c^2-1)^2 \quad \text{and} \quad G(\boldsymbol{d}) = \frac{1}{4\eta^2}(|\boldsymbol{d}|^2-1)^2; \tag{2.2}$$

and we represent their derivatives as $f(c) := F'(c)$ and $\boldsymbol{g}(\boldsymbol{d}) := G'(\boldsymbol{d})$.

Remark 2.1
Although the functionals $F(c)$ and $G(\boldsymbol{d})$ look similar, their role and their physical meanings are different. The functional $G(\boldsymbol{d})$ comes from the penalization of the constraint $|\boldsymbol{d}| = 1$; that is, it is classical in the nematic liquid crystal framework; on the other hand, $F(c)$ characterizes two different phases by its minima at $c = \pm 1$. There are other possible choices of the double-well potential like the logarithmic potential $F_{log} : (-1, 1) \to \boldsymbol{R}$ ([29])

$$F_{log}(c) = \frac{\theta}{2}[(1+c)\log(1+c) + (1-c)\log(1-c)] + \frac{\theta_c}{2}(1+c)(1-c), \tag{2.3}$$

where θ, θ_c are positive constants with $\theta_c > \theta$. It follows that F_{log} has a double-well form with minima at $c = \pm\beta$ (binodal points) for some $\beta < 1$ (close to 1 in the case of θ_c much larger than θ). Near $c = 0$, this potential leads to the usual approximation of the free energy as quartic polynomial given by $F(c)$. In contrast with the quartic approximation, the derivatives of F_{log} become unbounded at $c = \pm 1$. The results presented in the paper can be trivially extended to this type of logarithmic functional by using a truncated potential of F_{log} similarly to the truncated potential of F given in (3.19).

The functional $I(c) \in [0, 1]$ represents the volume fraction of liquid crystal, and its derivative will be denoted by $i(c) := I'(c)$. This functional could take different definitions always satisfying the following properties:

- $I \in C^2(\mathbb{R})$,
- $I(c) = 0$ if $c \leqslant -1$,
- $I(c) = 1$ if $c \geqslant 1$,
- $I(c) \in (0, 1)$ if $c \in (-1, 1)$.

For instance, we will consider the following interpolation function (Figure 2):

$$I(c) := \begin{cases} \dfrac{1}{16}(c+1)^3(3c^2-9c+8) & \text{if } c \in (-1,1)\,, \\ 1 & \text{if } c \geqslant 1\,, \\ 0 & \text{if } c \leqslant -1\,; \end{cases} \tag{2.4}$$

and its derivative is defined as

$$i(c) := I'(c) = \begin{cases} \dfrac{15}{16}(c+1)^2(c-1)^2 & \text{if } c \in (-1,1)\,, \\ 0 & \text{otherwise}\,. \end{cases}$$

It is known that for the three systems that we are combining in our formulation (namely, isotropic Newtonian fluid, nematic liquid crystal, and phase-field model), their governing equations satisfy a dissipative energy law. In fact, when each system is isolated, they have the 'dissipative energy laws':

- *Navier–Stokes model*

$$\frac{d}{dt}E_{kin}(\boldsymbol{u}) + 2\int_\Omega \nu|\boldsymbol{D}\boldsymbol{u}|^2 d\boldsymbol{x} = 0\,,$$

where $\boldsymbol{D}\boldsymbol{u} := (\nabla\boldsymbol{u} + \nabla\boldsymbol{u}^t)/2$ and $\nu > 0$ denotes the dynamic viscosity coefficient.

DOI: 10.1002/nme

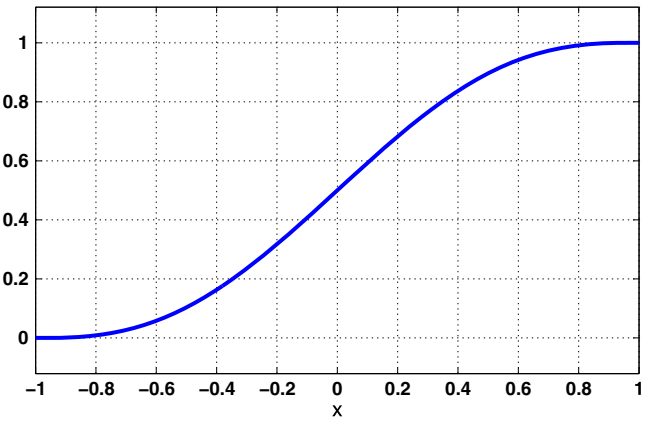

Figure 2. Interpolator $I(c)$ in interval $[0,1]$.

- *Cahn–Hilliard model*

$$\frac{d}{dt}E_{mix}(c)+\int_\Omega \gamma_{mix}\left|\nabla\frac{\delta E_{mix}}{\delta c}\right|^2 d\boldsymbol{x}=0\,,$$

  where $\gamma_{mix}>0$ represents the mobility coefficient.
- *Nematic liquid crystal model*

$$\frac{d}{dt}\left[E_{kin}(\boldsymbol{u})+\lambda_{nem}E_{nem}(\boldsymbol{d},c)\right]+2\int_\Omega \nu|\boldsymbol{D}\boldsymbol{u}|^2 d\boldsymbol{x}+\int_\Omega \gamma_{nem}\left|\frac{\delta E_{tot}}{\delta \boldsymbol{d}}\right|^2 d\boldsymbol{x}=0\,,$$

  where $(\delta\cdot/\delta\boldsymbol{d})$ denotes the variational derivative with respect to $\boldsymbol{d}$ and $\gamma_{nem}>0$ is the relaxation time coefficient.

In general, $(\delta E/\delta\phi)$ denotes the identification with a function in Ω of the variational derivative operator of a certain functional E with respect to the variable ϕ, which is defined as

$$\int_\Omega \frac{\delta E}{\delta\phi}\,\bar{\phi}\,d\boldsymbol{x}=\left\langle\frac{\delta E}{\delta\phi},\bar{\phi}\right\rangle=\lim_{\tau\to 0}\frac{E(\phi+\tau\bar{\phi})-E(\phi)}{\tau},$$

for all regular with compact support functions $\bar{\phi}$.

Now, we are going to derive the coupled system. This can be carried out combining ideas from the least action principle and the maximum dissipation principle [12, 13], arriving at the following PDE system:

$$\begin{cases} \boldsymbol{u}_t+\boldsymbol{u}\cdot\nabla\boldsymbol{u}+\nabla p-\nabla\cdot\sigma_{tot}=\boldsymbol{0}\,,\\ \nabla\cdot\boldsymbol{u}=0\,,\\ \boldsymbol{d}_t+(\boldsymbol{u}\cdot\nabla)\boldsymbol{d}+\gamma_{nem}\left(\dfrac{\delta E_{tot}}{\delta\boldsymbol{d}}\right)=\boldsymbol{0}\,,\\ c_t+\boldsymbol{u}\cdot\nabla c-\nabla\cdot\left(\gamma_{mix}\nabla\dfrac{\delta E_{tot}}{\delta c}\right)=0\,. \end{cases}\tag{2.5}$$

The PDE system (2.5) is supplemented with the following initial and boundary conditions:

$$\begin{aligned} &\boldsymbol{u}|_{t=0}=\boldsymbol{u}_0,\quad \boldsymbol{d}|_{t=0}=\boldsymbol{d}_0,\quad c|_{t=0}=c_0 && \text{in }\Omega,\\ &\boldsymbol{u}|_{\partial\Omega}=\left(I(c)\nabla\boldsymbol{d}\right)\boldsymbol{n}|_{\partial\Omega}=\boldsymbol{0} && \text{in }(0,T),\\ &\left.\frac{\partial c}{\partial\boldsymbol{n}}\right|_{\partial\Omega}=\left.\left(\nabla\frac{\delta E_{tot}}{\delta c}\right)\cdot\boldsymbol{n}\right|_{\partial\Omega}=0 && \text{in }(0,T), \end{aligned}\tag{2.6}$$

DOI: 10.1002/nme

where $\boldsymbol{n}$ denotes the outwards normal vector to the boundary $\partial\Omega$. The expressions for the identification function for each variational derivative in (2.5) will be introduced as two new variables,

$$\begin{aligned} \boldsymbol{w} &:= \frac{\delta E_{tot}}{\delta \boldsymbol{d}} = \lambda_{nem}\frac{\delta E_{nem}}{\delta \boldsymbol{d}} + \lambda_{anch}\frac{\delta E_{anch}}{\delta \boldsymbol{d}} \\ &= \lambda_{nem}\left(-\nabla\cdot(I(c)\nabla \boldsymbol{d}) + I(c)\,\boldsymbol{g}(\boldsymbol{d})\right) + \lambda_{anch}\frac{\delta E_{anch}}{\delta \boldsymbol{d}}\,, \end{aligned} \tag{2.7}$$

and

$$\begin{aligned} \mu &:= \frac{\delta E_{tot}}{\delta c} = \lambda_{mix}\frac{\delta E_{mix}}{\delta c} + \lambda_{nem}\frac{\delta E_{nem}}{\delta c} + \lambda_{anch}\frac{\delta E_{anch}}{\delta c} \\ &= \lambda_{mix}\left(-\Delta c + f(c)\right) + \lambda_{nem}I'(c)\left(\frac{1}{2}|\nabla \boldsymbol{d}|^2 + G(\boldsymbol{d})\right) + \lambda_{anch}\frac{\delta E_{anch}}{\delta c}, \end{aligned} \tag{2.8}$$

where the anchoring terms will depend on each of the following cases:

$$\frac{\delta E_{anch}}{\delta \boldsymbol{d}} = \begin{cases} 0 & \text{no anchoring}\,, \\ (\boldsymbol{d}\cdot\nabla c)\,\nabla c & \text{parallel anch.}\,, \\ |\nabla c|^2\boldsymbol{d} - (\boldsymbol{d}\cdot\nabla c)\,\nabla c & \text{homeotropic anch.}\,. \end{cases} \tag{2.9}$$

and

$$\frac{\delta E_{anch}}{\delta c} = \begin{cases} 0 & \text{no anchoring}\,, \\ -\nabla\cdot[(\boldsymbol{d}\cdot\nabla c)\,\boldsymbol{d}] & \text{parallel anch.}\,, \\ -\nabla\cdot[|\boldsymbol{d}|^2\nabla c - (\boldsymbol{d}\cdot\nabla c)\,\boldsymbol{d}] & \text{homeotropic anch.} \end{cases} \tag{2.10}$$

Finally, the stress tensor of the coupled system (2.5) reads

$$\sigma_{tot} = \sigma_{vis} + \sigma_{mix} + \sigma_{nem} + \sigma_{anch}\,,$$

where

$$\begin{aligned} \sigma_{vis} &= 2\,\nu\,\boldsymbol{D}\boldsymbol{u} && \text{in } \Omega\times(0,T), \\ \sigma_{mix} &= -\lambda_{mix}\nabla c\otimes\nabla c && \text{in } \Omega\times(0,T), \end{aligned} \tag{2.11}$$

$$\sigma_{nem} = -\lambda_{nem}I(c)(\nabla \boldsymbol{d})^t\nabla \boldsymbol{d} \quad \text{in } \Omega\times(0,T), \tag{2.12}$$

and

$$(\sigma_{anch})_{ij} = \lambda_{anch}\begin{cases} 0 & \text{no anchoring}, \\ -(\boldsymbol{d}\cdot\nabla c)\;(\nabla c\otimes \boldsymbol{d}) & \text{parallel anch.}, \\ -|\boldsymbol{d}|^2\,\nabla c\otimes\nabla c + (\boldsymbol{d}\cdot\nabla c)\;(\nabla c\otimes \boldsymbol{d}) & \text{homeotropic anch.} \end{cases}$$

Hereafter, $\otimes$ denotes the tensorial product, for instance, $(\nabla c\otimes \boldsymbol{d})_{ij} = \partial_i c\, d_j$.

Remark 2.2
The viscosities of each component of the mixture could be different. In order to capture this possibility, we consider the coefficient ν depending on the phase function c; therefore, hereafter, we will denote $\nu(c)$ instead of ν, where $\nu(c)$ is a positive function.

The effect of the stress tensor $-\nabla\cdot\sigma_{tot}$ can be rewritten in order to arrive at a simpler formulation of the model, where these new terms are going to be easier to handle.

DOI: 10.1002/nme

Lemma 2.3 (Reformulation of the stress tensor)
It holds

$$-\nabla\cdot\sigma_{mix}-\nabla\cdot\sigma_{nem}-\nabla\cdot\sigma_{anch}=-\mu\,\nabla c-(\nabla \boldsymbol{d})^t\boldsymbol{w}+\nabla\varphi \text{ in } \Omega\times(0,T)\,, \tag{2.13}$$

where

$$\varphi=\lambda_{nem}\,I(c)\left(\frac{1}{2}\,|\nabla \boldsymbol{d}|^2+G(\boldsymbol{d})\right)+\lambda_{mix}\left(\frac{1}{2}\,|\nabla c|^2+F(c)\right)+\frac{\lambda_{anch}}{2}\,W(\boldsymbol{d},c)\,,$$

and

$$W(\boldsymbol{d},c)=\begin{cases}0 & \text{no anchoring,}\\ |\boldsymbol{d}\cdot\nabla c|^2 & \text{parallel anch.,}\\ \left(|\boldsymbol{d}|^2\,|\nabla c|^2-|\boldsymbol{d}\cdot\nabla c|^2\right) & \text{homeotropic anch.}\end{cases} \tag{2.14}$$

Proof
See Appendix. □

By applying Lemma 2.3 and using the variables $\boldsymbol{w}$ and μ, system (2.5) can be reformulated as

$$\begin{cases}\boldsymbol{u}_t+\boldsymbol{u}\cdot\nabla\boldsymbol{u}+\nabla\widetilde{p}-\nabla\cdot(2\nu(c)\boldsymbol{D}\boldsymbol{u})-\mu\,\nabla c-(\nabla\boldsymbol{d})^t\boldsymbol{w}=0\,,\\ \nabla\cdot\boldsymbol{u}=0\,,\\ \boldsymbol{d}_t+(\boldsymbol{u}\cdot\nabla)\boldsymbol{d}+\gamma_{nem}\boldsymbol{w}=0\,,\\ \lambda_{nem}[-\nabla\cdot(I(c)\nabla\boldsymbol{d})+I(c)\,\boldsymbol{g}(\boldsymbol{d})]+\lambda_{anch}\,\dfrac{\delta E_{anch}}{\delta\boldsymbol{d}}-\boldsymbol{w}=0\,,\\ c_t+\boldsymbol{u}\cdot\nabla c-\nabla\cdot(\gamma_{mix}\nabla\mu)=0\,,\\ \lambda_{mix}[-\Delta c+f(c)]+\lambda_{nem}I'(c)\left(\dfrac{1}{2}|\nabla\boldsymbol{d}|^2+G(\boldsymbol{d})\right)\\ \qquad+\lambda_{anch}\,\dfrac{\delta E_{anch}}{\delta c}-\mu=0\,,\end{cases} \tag{2.15}$$

where $(\delta E_{anch}/\delta\boldsymbol{d})$ and $(\delta E_{anch}/\delta c)$ were previously computed in (2.9) and (2.10), respectively, and the following modified potential appears:

$$\widetilde{p}:=p+\varphi\,.$$

Taking into account the equalities

$$\begin{cases}-\mu\nabla c=-\nabla(c\,\mu)+c\nabla\mu\,,\\ \boldsymbol{u}\cdot\nabla c=\nabla\cdot(c\,\boldsymbol{u})\,,\end{cases}$$

(in the second relation, the incompressibility constraint $\nabla\cdot\boldsymbol{u}=0$ has been used), we can redefine again the pressure term as

$$\widehat{p}:=\widetilde{p}-c\,\mu\,.$$

For simplicity of notation, we write in the following p instead of $\widehat{p}$.

Now, we formally deduce the two main properties of this problem, namely, the conservation of the total volume $\int_\Omega c(t,\boldsymbol{x})\,d\boldsymbol{x}$ and the dissipativity of the total energy E_{tot}.

By integrating Equation $(2.15)_5$ over Ω, we recover the conservation of volume (standard for Cahn–Hilliard models):

$$\frac{d}{dt}\int_\Omega c(t,\boldsymbol{x})\,d\boldsymbol{x}=0\,.$$

DOI: 10.1002/nme

On the other hand, multiplying $(2.15)_1$ by $\boldsymbol{u}$, $(2.15)_2$ by p, $(2.15)_3$ by $\boldsymbol{w}$, $(2.15)_4$ by $\boldsymbol{d}_t$, $(2.15)_5$ by μ, and $(2.15)_6$ by c_t, integrating over Ω, using the boundary conditions (2.6), accounting (2.7) and (2.8), and using the chain rule

$$\left(\frac{\delta E_{tot}}{\delta \boldsymbol{d}}, \boldsymbol{d}_t\right) + \left(\frac{\delta E_{tot}}{\delta c}, c_t\right) = \frac{d}{dt}\left[\lambda_{nem} E_{nem}(\boldsymbol{d}, c) + \lambda_{mix} E_{mix}(c) + \lambda_{anch}\, E_{anch}(\boldsymbol{d}, c)\right],$$

the following (dissipative) energy law holds:

$$\frac{d}{dt} E_{tot}(\boldsymbol{u}, \boldsymbol{d}, c) + 2\int_\Omega \nu |\boldsymbol{D}\boldsymbol{u}|^2 d\boldsymbol{x} + \gamma_{nem}\int_\Omega |\boldsymbol{w}|^2 d\boldsymbol{x} + \gamma_{mix}\int_\Omega |\nabla\mu|^2 d\boldsymbol{x} = 0. \tag{2.16}$$

In particular, this energy law implies the dissipative character of the free energy $E_{tot}(\boldsymbol{u}, \boldsymbol{d}, c)$ defined in (2.1) as the sum of the kinetic, mixing, elastic, and anchoring energies.

Remark 2.4
It is possible to consider other types of boundary conditions and still maintain an energy law like (2.16). Indeed, the same type of energy law can be derived changing the non-slip boundary conditions $\boldsymbol{u}|_{\partial\Omega} = 0$ by the slip-friction boundary conditions,

$$\boldsymbol{u}\cdot\boldsymbol{n}|_{\partial\Omega} = 0, \qquad \left[(\sigma_{tot}\boldsymbol{n})_{tg} - \alpha(\boldsymbol{u} - \boldsymbol{u}_{ext})_{tg}\right]\big|_{\partial\Omega} = \boldsymbol{0} \qquad \text{in } (0,T),$$

where tg denotes the tangential part to the boundary $\partial\Omega$, $\boldsymbol{u}_{ext}$ is the external velocity, and $\alpha \geqslant 0$ is a friction coefficient. The key point is to take into account the following relations:

$$\begin{array}{ll} \boldsymbol{u}\cdot\boldsymbol{n}|_{\partial\Omega} = 0 & \Rightarrow (\varphi\,\mathbb{I})_{tg}|_{\partial\Omega} = \mathbb{O}, \\ \nabla c\cdot\boldsymbol{n}|_{\partial\Omega} = 0 & \Rightarrow \sigma_{mix}\boldsymbol{n}|_{\partial\Omega} = \boldsymbol{0}, \\ (I(c)\nabla\boldsymbol{d})\,\boldsymbol{n}|_{\partial\Omega} = \boldsymbol{0} & \Rightarrow \sigma_{nem}\boldsymbol{n}|_{\partial\Omega} = \boldsymbol{0}, \\ \nabla c\cdot\boldsymbol{n}|_{\partial\Omega} = 0 & \Rightarrow \sigma_{anch}\boldsymbol{n}|_{\partial\Omega} = \boldsymbol{0}, \end{array}$$

where $\mathbb{I}$ and $\mathbb{O}$ denote the identity and null matrix, respectively. In fact, it holds

$$\sigma_{tot}\boldsymbol{n}\,|_{\partial\Omega} = \sigma_{vis}\boldsymbol{n}\,|;$$

hence, the energy law can be directly deduced.

From energy law (2.16), we deduce the following regularity for a (possible) solution:

$$\begin{cases} \boldsymbol{u} \in L^\infty(0,T;\mathbf{L}^2(\Omega)) \cap L^2(0,T;\mathbf{H}^1(\Omega)), \\ \boldsymbol{w} \in L^2(0,T;\mathbf{L}^2(\Omega)), \\ \nabla c \in L^\infty(0,T;\mathbf{L}^2(\Omega)), \qquad \nabla\mu \in L^2(0,T;\mathbf{L}^2(\Omega)), \\ \int_\Omega F(c)d\boldsymbol{x} \in L^\infty(0,T), \\ \int_\Omega I(c)\left(\frac{1}{2}|\nabla\boldsymbol{d}|^2 + G(\boldsymbol{d})\right)d\boldsymbol{x} \in L^\infty(0,T) \\ E_{anch}(c,\boldsymbol{d}) \in L^\infty(0,T). \end{cases} \tag{2.17}$$

In particular, from $\int_\Omega F(c)d\boldsymbol{x} \in L^\infty(0,T)$ and $\int_\Omega I(c)\,G(\boldsymbol{d})\,d\boldsymbol{x} \in L^\infty(0,T)$, and the inequalities

$$F(c) \geqslant \frac{1}{8\varepsilon^2}\left(c^4 - 2\right), \quad G(\boldsymbol{d}) \geqslant \frac{1}{8\eta^2}\left(|\boldsymbol{d}|^4 - 2\right),$$

we can deduce the estimates

$$c \in L^\infty(0,T;H^1(\Omega)), \quad \int_\Omega I(c)\,|\boldsymbol{d}|^4 \in L^\infty(0,T). \tag{2.18}$$

DOI: 10.1002/nme

Remark 2.5
In order to obtain a regularity result for $\boldsymbol{d}$ in the whole domain Ω, we can multiply $(2.15)_3$ by $\boldsymbol{d}$ in and $(2.15)_4$ by $\boldsymbol{d}$, arriving at

$$\frac{1}{2}\frac{d}{dt}\int_\Omega |\boldsymbol{d}|^2 + \gamma_{nem}\int_\Omega \boldsymbol{w}\cdot\boldsymbol{d} = 0. \tag{2.19}$$

On the other hand, testing $(2.15)_4$ by $\boldsymbol{d}$,

$$\int_\Omega \boldsymbol{w}\cdot\boldsymbol{d} = \lambda_{nem}\int_\Omega I(c)\,|\nabla\boldsymbol{d}|^2\,d\boldsymbol{x} + \lambda_{nem}\int_\Omega I(c)\,g(\boldsymbol{d})\cdot\boldsymbol{d}\,d\boldsymbol{x} + \lambda_{anch}\int_\Omega \frac{\delta E_{anch}}{\delta \boldsymbol{d}}\cdot\boldsymbol{d}. \tag{2.20}$$

Notice that $\displaystyle\int_\Omega I(c)\,|\nabla\boldsymbol{d}|^2\,d\boldsymbol{x} \geqslant 0$ and

$$\int_\Omega \frac{\delta E_{anch}}{\delta \boldsymbol{d}}\cdot\boldsymbol{d} = \left\{\begin{array}{ll} 0 & \text{no anchoring,}\\ \int_\Omega |\boldsymbol{d}\cdot\nabla c|^2 & \text{parallel anchoring,}\\ \int_\Omega |\nabla c|^2|\boldsymbol{d}|^2 - |\boldsymbol{d}\cdot\nabla c|^2 & \text{homeotropic anchoring.}\end{array}\right\} = 2\,E_{anch}(c,\boldsymbol{d}) \geqslant 0.$$

In order to bound the second term of (2.20), taking into account that

$$g(\boldsymbol{d})\cdot\boldsymbol{d} = \left\{\begin{array}{l} \dfrac{2}{\eta^2}\,(|\boldsymbol{d}|-1)\,|\boldsymbol{d}|^2 \text{ if } |\boldsymbol{d}|\geqslant 1,\\[2ex] \dfrac{2}{\eta^2}\,(|\boldsymbol{d}|^2-1)\,|\boldsymbol{d}|^2 \text{ if } |\boldsymbol{d}|\leqslant 1,\end{array}\right.$$

then one has $\displaystyle\int_\Omega I(c)\,g(\boldsymbol{d})\cdot\boldsymbol{d} \geqslant 0$ if $|\boldsymbol{d}|\geqslant 1$, and the term $\displaystyle\frac{2}{\eta^2}\int_\Omega I(c)\,|\boldsymbol{d}|^2$ can be bounded on the right-hand side if $|\boldsymbol{d}|\leqslant 1$. In fact, because $I(c)\leqslant 1$,

$$\lambda_{nem}\frac{2}{\eta^2}\int_\Omega I(c)\,|\boldsymbol{d}|^2 \leqslant \lambda_{nem}\frac{2}{\eta^2}\int_\Omega |\boldsymbol{d}|^2.$$

Then, (2.19) and (2.20) yield

$$\frac{1}{2}\frac{d}{dt}\int_\Omega |\boldsymbol{d}|^2 \leqslant \lambda_{nem}\frac{2}{\eta^2}\int_\Omega |\boldsymbol{d}|^2;$$

hence, using the Gronwall's lemma, we arrive at

$$\boldsymbol{d}\in L^\infty(0,T;\mathbf{L}^2(\Omega)). \tag{2.21}$$

3. NUMERICAL SCHEMES

The purpose of this section is to design efficient numerical schemes for model (2.15). We are interested in using finite element approximations in space and finite differences in time, while the resulting scheme satisfies the conservation of $\int_\Omega c$ and a discrete version of continuous energy law (2.16). To this end, we present a first order in time, one-step, linear unconditionally energy-stable (see the concept of energy stability in Definition 3.1 in the succeeding text) numerical scheme that combines ideas for approximating linearly the potentials $f(c)$, $i(c)$, and $\boldsymbol{g}(\boldsymbol{d})$ with splitting ideas

DOI: 10.1002/nme

to decouple the computation of the fluid part from the phase-field one and from the nematic part maintaining the energy stability. Let $\boldsymbol{V}_h \times P_h \times \boldsymbol{D}_h \times \boldsymbol{W}_h \times C_h \times M_h$ be conformed finite element spaces in $\boldsymbol{H}^1_0(\Omega) \times L^2_0(\Omega) \times \boldsymbol{H}^1(\Omega) \times \boldsymbol{L}^2(\Omega) \times H^1(\Omega) \times H^1(\Omega)$ corresponding to a regular and quasi-uniform triangulation $\mathcal{T}_h$ of the domain Ω with polyhedric boundary $\partial\Omega$. For the sake of simplicity, we skip the use of the subscript h to denote functions that are discrete in space. For simplicity, we describe the time discretization using a uniform partition of the time interval $[0, T]$: $t_n = nk$, where $k = T/N$ denotes the (fixed) time step. In general, given $(\boldsymbol{u}^n, p^n, \boldsymbol{d}^n, \boldsymbol{w}^n, c^n, \mu^n)$, an approximation of a regular enough solution (if it exists) at $t = t_n$, we have to compute $(\boldsymbol{u}^{n+1}, p^{n+1}, \boldsymbol{d}^{n+1}, \boldsymbol{w}^{n+1}, c^{n+1}, \mu^{n+1})$ as an approximation at $t = t_{n+1}$.

We recall here the concept of energy stability already introduced for other energy-based systems [3, 18, 30, 31].

Definition 3.1
A numerical scheme is energy stable if it holds

$$\begin{aligned}\delta_t E_{tot}(\boldsymbol{u}^{n+1}, \boldsymbol{d}^{n+1}, c^{n+1}) + 2\int_\Omega \nu(c^{n+1})|\boldsymbol{D}\boldsymbol{u}^{n+1}|^2 d\boldsymbol{x} + \gamma_{nem}\int_\Omega |\boldsymbol{w}^{n+1}|^2 d\boldsymbol{x} \\ +\gamma_{mix}\int_\Omega |\nabla\mu^{n+1}|^2 d\boldsymbol{x} \leqslant 0 \quad \forall\, n\,.\end{aligned} \tag{3.1}$$

In particular, energy-stable schemes satisfy the energy decreasing in time property

$$E_{tot}(\boldsymbol{u}^{n+1}, \boldsymbol{d}^{n+1}, c^{n+1}) \leqslant E_{tot}(\boldsymbol{u}^n, \boldsymbol{d}^n, c^n) \quad \forall\, n\,.$$

Hereafter, we denote the discrete time derivative as

$$\delta_t a^{n+1} := \frac{a^{n+1} - a^n}{k}.$$

3.1. Description of the scheme

3.1.1. A coupled nonlinear first-order implicit scheme. The first idea that comes to mind to approximate problem (2.15) is to develop an implicit scheme such that as follows: Let $(\boldsymbol{u}^n, p^n, \boldsymbol{d}^n, \boldsymbol{w}^n, c^n, \mu^n) \in \boldsymbol{V}_h \times P_h \times \boldsymbol{D}_h \times \boldsymbol{W}_h \times C_h \times M_h$ be known and
find $(\boldsymbol{u}^{n+1}, p^{n+1}, \boldsymbol{d}^{n+1}, \boldsymbol{w}^{n+1}, c^{n+1}, \mu^{n+1})$ satisfying the following discrete variational problem,

$$\left\{\begin{aligned}
\left(\frac{\boldsymbol{u}^{n+1} - \boldsymbol{u}^n}{k}, \bar{\boldsymbol{u}}\right) + \big((\boldsymbol{u}^{n+1}\cdot\nabla)\boldsymbol{u}^{n+1}, \bar{\boldsymbol{u}}\big) - (p^{n+1}, \nabla\cdot\bar{\boldsymbol{u}}) + 2(\nu\boldsymbol{D}\boldsymbol{u}^{n+1}, \boldsymbol{D}\bar{\boldsymbol{u}}) \\
- \big((\nabla\boldsymbol{d}^{n+1})^t\boldsymbol{w}^{n+1}, \bar{\boldsymbol{u}}\big) + (c^{n+1}\nabla\mu^{n+1}, \bar{\boldsymbol{u}}) = 0\,, \\
(\nabla\cdot\boldsymbol{u}^{n+1}, \bar{p}) = 0\,, \\
\left(\frac{\boldsymbol{d}^{n+1} - \boldsymbol{d}^n}{k}, \bar{\boldsymbol{w}}\right) + \big((\boldsymbol{u}^{n+1}\cdot\nabla)\boldsymbol{d}^{n+1}, \bar{\boldsymbol{w}}\big) + \gamma_{nem}(\boldsymbol{w}^{n+1}, \bar{\boldsymbol{w}}) = 0\,, \\
\lambda_{nem}(I(c^{n+1})\nabla\boldsymbol{d}^{n+1}, \nabla\bar{\boldsymbol{d}}) + \lambda_{nem}(I(c^{n+1})\,\boldsymbol{g}(\boldsymbol{d}^{n+1}), \bar{\boldsymbol{d}}) \\
+\lambda_{anch}\left(\frac{\delta E_{anch}}{\delta\boldsymbol{d}}(c^{n+1}, \boldsymbol{d}^{n+1}), \bar{\boldsymbol{d}}\right) - (\boldsymbol{w}^{n+1}, \bar{\boldsymbol{d}}) = 0\,, \\
\left(\frac{c^{n+1} - c^n}{k}, \bar{\mu}\right) - (c^{n+1}\,\boldsymbol{u}^{n+1}, \nabla\bar{\mu}) + \gamma_{mix}(\nabla\mu^{n+1}, \nabla\bar{\mu}) = 0\,, \\
\lambda_{mix}(\nabla c^{n+1}, \nabla\bar{c}) + \lambda_{mix}(f(c^{n+1}), \bar{c}) + \lambda_{nem}\left(i(c^{n+1})\left[\frac{|\nabla\boldsymbol{d}^{n+1}|^2}{2} + G(\boldsymbol{d}^{n+1})\right], \bar{c}\right) \\
+\lambda_{anch}\left(\frac{\delta E_{anch}}{\delta c}(c^{n+1}, \boldsymbol{d}^{n+1}), \bar{c}\right) - (\mu^{n+1}, \bar{c}) = 0\,,
\end{aligned}\right. \tag{3.2}$$

for each $(\bar{\boldsymbol{u}}, \bar{p}, \bar{\boldsymbol{w}}, \bar{\boldsymbol{d}}, \bar{\mu}, \bar{c}) \in \boldsymbol{V}_h \times P_h \times \boldsymbol{W}_h \times \boldsymbol{D}_h \times M_h \times C_h$. Hereafter, $(\cdot,\cdot)$ denotes the inner product in $L^2(\Omega)$, and $\|\cdot\|_{L^2}$ denotes the corresponding $L^2(\Omega)$-norm.

DOI: 10.1002/nme

The main disadvantages of this approach are that the computational cost of using scheme (3.2) is very high because all the equations are coupled, it is not clear that any iterative method to approximate the nonlinear scheme will converge because of the several nonlinearities in the system, and it is not known if this scheme will satisfy a discrete version of energy law (2.16) to assure the energy stability.

3.1.2. Splitting in time schemes. Our aim is to design efficient and accurate numerical schemes to approximate (2.15). The main advantage of our work is to design linear schemes that decouple the computation of the complete system into smaller sub-systems, maintaining the energy stability via a discrete version of the energy law (2.16).

We have found two possibilities to decouple computations for nematic part $(\boldsymbol{d}^{n+1}, \boldsymbol{w}^{n+1})$ from the phase-field part (c^{n+1}, μ^{n+1}) and from the fluid part $(\boldsymbol{u}^{n+1}, p^{n+1})$. In the following, we will detail both numerical schemes, but we will show in detail the energy stability just for one of the proposed schemes, because energy stability of the second scheme can be obtained just applying the same ideas.

3.1.3. $\boldsymbol{d}$-c-$\boldsymbol{u}$ scheme. Let $(\boldsymbol{u}^n, p^n, \boldsymbol{d}^n, \boldsymbol{w}^n, c^n, \mu^n) \in \boldsymbol{V}_h \times P_h \times \boldsymbol{D}_h \times \boldsymbol{W}_h \times C_h \times M_h$ be known.

Step 1
Find $(\boldsymbol{d}^{n+1}, \boldsymbol{w}^{n+1}) \in \boldsymbol{D}_h \times \boldsymbol{W}_h$ such that, for each $(\bar{\boldsymbol{d}}, \bar{\boldsymbol{w}}) \in \boldsymbol{D}_h \times \boldsymbol{W}_h$,

$$\left\{\begin{array}{l} \left(\dfrac{\boldsymbol{d}^{n+1}-\boldsymbol{d}^n}{k}, \bar{\boldsymbol{w}}\right) + ((\boldsymbol{u}^\star \cdot \nabla)\boldsymbol{d}^n, \bar{\boldsymbol{w}}) + \gamma_{nem}(\boldsymbol{w}^{n+1}, \bar{\boldsymbol{w}}) = 0\,, \\ \lambda_{nem}\left(I(c^n)\nabla \boldsymbol{d}^{n+1}, \nabla \bar{\boldsymbol{d}}\right) + \lambda_{nem}\left(I(c^n)\boldsymbol{g}_k(\boldsymbol{d}^{n+1}, \boldsymbol{d}^n), \bar{\boldsymbol{d}}\right) \\ \qquad\qquad +\lambda_{anch}\left(\Lambda_{\boldsymbol{d}}(\boldsymbol{d}^{n+1}, c^n), \bar{\boldsymbol{d}}\right) - (\boldsymbol{w}^{n+1}, \bar{\boldsymbol{d}}) = 0\,, \end{array}\right. \tag{3.3}$$

where

$$\boldsymbol{u}^\star := \boldsymbol{u}^n + 2\,k\,(\nabla \boldsymbol{d}^n)^t \boldsymbol{w}^{n+1}\,, \tag{3.4}$$

$\boldsymbol{g}_k(\boldsymbol{d}^{n+1}, \boldsymbol{d}^n)$ denotes a first-order approximation of $\boldsymbol{g}(\boldsymbol{d}(t_{n+1}))$, and $\Lambda_{\boldsymbol{d}}(\boldsymbol{d}^{n+1}, c^n)$ represents a first-order approximation of $\dfrac{\delta E_{anch}}{\delta \boldsymbol{d}}(\boldsymbol{d}(t_{n+1}), c(t_{n+1}))$:

$$\Lambda_{\boldsymbol{d}}(\boldsymbol{d}, c) := \frac{\delta E_{anch}}{\delta \boldsymbol{d}}(\boldsymbol{d}, c) = \delta_1 |\nabla c|^2\, \boldsymbol{d} + \delta_2\,(\boldsymbol{d} \cdot \nabla c)\,\nabla c\,, \tag{3.5}$$

where (δ_1, δ_2) will take different forms depending on the anchoring effect, that is,

$$(\delta_1, \delta_2) = \left\{\begin{array}{ll} (0,0) & \text{no anchoring,} \\ (0,1) & \text{parallel anch.,} \\ (1,-1) & \text{homeotropic anch.} \end{array}\right. \tag{3.6}$$

Step 2
Find $(c^{n+1}, \mu^{n+1}) \in C_h \times M_h$ such that, for each $(\bar{c}, \bar{\mu}) \in C_h \times M_h$,

$$\left\{\begin{array}{l} \left(\dfrac{c^{n+1}-c^n}{k}, \bar{\mu}\right) - (c^n \boldsymbol{u}^{\star\star}, \nabla \bar{\mu}) + \gamma_{mix}(\nabla \mu^{n+1}, \nabla \bar{\mu}) = 0\,, \\ \qquad \lambda_{mix}(\nabla c^{n+1}, \nabla \bar{c}) + \lambda_{mix}(f_k(c^{n+1}, c^n), \bar{c}) \\ +\lambda_{nem}\left(i_k(c^{n+1}, c^n)\left[\dfrac{1}{2}|\nabla \boldsymbol{d}^{n+1}|^2 + G(\boldsymbol{d}^{n+1})\right], \bar{c}\right) \\ \qquad +\lambda_{anch}\left(\Lambda_c(\boldsymbol{d}^{n+1}, c^{n+1}), \nabla \bar{c}\right) - (\mu^{n+1}, \bar{c}) = 0\,, \end{array}\right. \tag{3.7}$$

where

$$\boldsymbol{u}^{\star\star} := \boldsymbol{u}^n - 2\,k\,c^n \nabla \mu^{n+1}\,, \tag{3.8}$$

DOI: 10.1002/nme

$f_k(c^{n+1}, c^n)$ denotes a first-order approximation of $f(c(t_{n+1}))$, and $-\nabla \cdot (\Lambda_c(\boldsymbol{d}, c)) = \dfrac{\delta E_{anch}}{\delta c}(\boldsymbol{d}, c)$, that is,

$$\Lambda_c(\boldsymbol{d}, c) = \delta_1 |\boldsymbol{d}|^2 \nabla c + \delta_2 (\boldsymbol{d} \cdot \nabla c)\, \boldsymbol{d}\,, \tag{3.9}$$

where the values of (δ_1, δ_2) are defined in (3.6), which depend on the type of anchoring.

Step 3
Find $(\boldsymbol{u}^{n+1}, p^{n+1}) \in \boldsymbol{V}_h \times P_h$ such that, for each $(\bar{\boldsymbol{u}}, \bar{p}) \in \boldsymbol{V}_h \times P_h$,

$$\begin{cases} \left(\dfrac{\boldsymbol{u}^{n+1} - \widehat{\boldsymbol{u}}}{k}, \bar{\boldsymbol{u}}\right) + c(\boldsymbol{u}^n, \boldsymbol{u}^{n+1}, \bar{\boldsymbol{u}}) - (p^{n+1}, \nabla \cdot \bar{\boldsymbol{u}}) \\ \qquad\qquad +2\,(\nu(c^{n+1})\boldsymbol{D}\boldsymbol{u}^{n+1}, \boldsymbol{D}\bar{\boldsymbol{u}}) = 0\,, \\ \qquad\qquad (\nabla \cdot \boldsymbol{u}^{n+1}, \bar{p}) = 0\,, \end{cases} \tag{3.10}$$

where

$$\widehat{\boldsymbol{u}} := \frac{\boldsymbol{u}^\star + \boldsymbol{u}^{\star\star}}{2}\,. \tag{3.11}$$

It is easy to deduce, taking $\bar{\mu} = 1$ in step 2, the conservation property of the scheme:

$$\int_\Omega c^{n+1}\, d\boldsymbol{x} = \int_\Omega c^n\, d\boldsymbol{x}. \tag{3.12}$$

On the other hand, the following result gives a local in time discrete energy law, which will be the first step to prove the energy stability of the scheme.

Theorem 3.2
Schemes (3.3)–(3.11) satisfy the following local in time discrete energy law:

$$\begin{aligned} \delta_t E(\boldsymbol{d}^{n+1}, c^{n+1}, \boldsymbol{u}^{n+1}) &+ \gamma_{nem} \|\boldsymbol{w}^{n+1}\|_{L^2}^2 + \gamma_{mix} \|\nabla \mu^{n+1}\|_{L^2}^2 + 2\,\|\nu(c^{n+1})^{1/2} \boldsymbol{D}\boldsymbol{u}^{n+1}\|_{L^2}^2 \\ &+ ND_{\boldsymbol{u}}^{n+1} + ND_{elast}^{n+1}(c^n) + ND_{penal}^{n+1}(c^n) + ND_{philic}^{n+1} \\ &+ ND_{phobic}^{n+1} + ND_{interp}^{n+1}(\boldsymbol{d}^{n+1}) + ND_{anch}^{n+1} = 0, \end{aligned} \tag{3.13}$$

where the numerical dissipation terms are

$$\begin{cases} ND_{\boldsymbol{u}}^{n+1} = \frac{1}{2k}\left(\|\boldsymbol{u}^{n+1} - \widehat{\boldsymbol{u}}\|_{L^2}^2 + \frac{\|\widehat{\boldsymbol{u}} - \boldsymbol{u}^\star\|_{L^2}^2 + \|\widehat{\boldsymbol{u}} - \boldsymbol{u}^{\star\star}\|_{L^2}^2}{2} \right. \\ \qquad\qquad \left. + \frac{\|\boldsymbol{u}^\star - \boldsymbol{u}^n\|_{L^2}^2 + \|\boldsymbol{u}^{\star\star} - \boldsymbol{u}^n\|_{L^2}^2}{2}\right), \\ ND_{elast}^{n+1}(c) = \lambda_{nem} \dfrac{k}{2} \displaystyle\int_\Omega I(c)\, \left|\delta_t \nabla \boldsymbol{d}^{n+1}\right|^2 d\boldsymbol{x}, \\ ND_{penal}^{n+1}(c) = \lambda_{nem} \displaystyle\int_\Omega I(c)\, \left(\boldsymbol{g}_k(\boldsymbol{d}^{n+1}, \boldsymbol{d}^n) \cdot \delta_t \boldsymbol{d}^{n+1} - \delta_t G(\boldsymbol{d}^{n+1})\right) d\boldsymbol{x}, \\ ND_{philic}^{n+1} = \lambda_{mix} \dfrac{k}{2} \displaystyle\int_\Omega \left|\delta_t \nabla c^{n+1}\right|^2 d\boldsymbol{x}, \\ ND_{phobic}^{n+1} = \lambda_{mix} \displaystyle\int_\Omega \left(f_k(c^{n+1}, c^n)\, \delta_t c^{n+1} - \delta_t F(c^{n+1})\right) d\boldsymbol{x}, \\ ND_{interp}^{n+1}(\boldsymbol{d}) = \lambda_{nem} \displaystyle\int_\Omega \left(\frac{|\nabla \boldsymbol{d}|^2}{2} + G(\boldsymbol{d})\right) \\ \qquad\qquad \times \left(i_k(c^{n+1}, c^n)\, \delta_t c^{n+1} - \delta_t I(c^{n+1})\right) d\boldsymbol{x}, \end{cases} \tag{3.14}$$

DOI: 10.1002/nme

and

$$ND_{anch}^{n+1} = \lambda_{anch}\frac{k}{2}\int_\Omega \left[\delta_1\left(|\delta_t \boldsymbol{d}^{n+1}|^2|\nabla c^n|^2 + |\boldsymbol{d}^{n+1}|^2|\delta_t \nabla c^{n+1}|^2\right)\right. \\ \left. + \delta_2\left(|\delta_t \boldsymbol{d}^{n+1}\cdot\nabla c^n|^2 + |\boldsymbol{d}^{n+1}\cdot\nabla \delta_t c^{n+1}|^2\right)\right] d\boldsymbol{x},$$

with the values of (δ_1, δ_2) depending on the type of anchoring defined in (3.6).

Proof
See Appendix. □

Remark 3.3
In practice, for the numerical computations, there is no need to introduce the extra unknowns $\boldsymbol{u}^\star$, $\boldsymbol{u}^{\star\star}$, and $\widehat{\boldsymbol{u}}$; they are only used as a tool to show the energy stability of the scheme.

3.1.4. c-d-u scheme. Let $(\boldsymbol{u}^n, p^n, \boldsymbol{d}^n, \boldsymbol{w}^n, c^n, \mu^n) \in \boldsymbol{V}_h \times P_h \times \boldsymbol{D}_h \times \boldsymbol{W}_h \times C_h \times M_h$ be known.
Step 1: Find $(c^{n+1}, \mu^{n+1}) \in C_h \times M_h$ such that, for each $(\bar{c}, \bar{\mu}) \in C_h \times M_h$,

$$\begin{cases} \left(\dfrac{c^{n+1}-c^n}{k}, \bar{\mu}\right) - (c^n \boldsymbol{u}^{\star\star}, \nabla\bar{\mu}) + \gamma_{mix}(\nabla\mu^{n+1}, \nabla\bar{\mu}) = 0, \\ \lambda_{mix}(\nabla c^{n+1}, \nabla\bar{c}) + \lambda_{mix}(f_k(c^{n+1}, c^n), \bar{c}) \\ +\lambda_{nem}\left(i_k(c^{n+1}, c^n)\left[\dfrac{1}{2}|\nabla \boldsymbol{d}^n|^2 + G(\boldsymbol{d}^n)\right], \bar{c}\right) \\ +\lambda_{anch}\left(\Lambda_c(\boldsymbol{d}^n, c^{n+1}), \nabla\bar{c}\right) - (\mu^{n+1}, \bar{c}) = 0, \end{cases} \tag{3.15}$$

where $\boldsymbol{u}^{\star\star}$ and $\Lambda_c(\boldsymbol{d}, c)$ are defined in (3.8) and (3.9), respectively.
Step 2: Find $(\boldsymbol{d}^{n+1}, \boldsymbol{w}^{n+1}) \in \boldsymbol{D}_h \times \boldsymbol{W}_h$ such that, for each $(\bar{\boldsymbol{d}}, \bar{\boldsymbol{w}}) \in \boldsymbol{D}_h \times \boldsymbol{W}_h$,

$$\begin{cases} \left(\dfrac{\boldsymbol{d}^{n+1}-\boldsymbol{d}^n}{k}, \bar{\boldsymbol{w}}\right) + ((\boldsymbol{u}^\star\cdot\nabla)\boldsymbol{d}^n, \bar{\boldsymbol{w}}) + \gamma_{nem}(\boldsymbol{w}^{n+1}, \bar{\boldsymbol{w}}) = 0, \\ \lambda_{nem}\left(I(c^{n+1})\nabla\boldsymbol{d}^{n+1}, \nabla\bar{\boldsymbol{d}}\right) + \lambda_{nem}\left(I(c^{n+1})\boldsymbol{g}_k(\boldsymbol{d}^{n+1}, \boldsymbol{d}^n), \bar{\boldsymbol{d}}\right) \\ +\lambda_{anch}\left(\Lambda_{\boldsymbol{d}}(\boldsymbol{d}^{n+1}, c^{n+1}), \bar{\boldsymbol{d}}\right) - (\boldsymbol{w}^{n+1}, \bar{\boldsymbol{d}}) = 0, \end{cases} \tag{3.16}$$

where $\boldsymbol{u}^\star$ and $\Lambda_{\boldsymbol{d}}(\boldsymbol{d}, c)$ are defined in (3.4) and (3.5), respectively.
Step 3: Find $(\boldsymbol{u}^{n+1}, p^{n+1}) \in \boldsymbol{V}_h \times P_h$ such that, for each $(\bar{\boldsymbol{u}}, \bar{p}) \in \boldsymbol{V}_h \times P_h$,

$$\begin{cases} \left(\dfrac{\boldsymbol{u}^{n+1}-\widehat{\boldsymbol{u}}}{k}, \bar{\boldsymbol{u}}\right) + c(\boldsymbol{u}^n, \boldsymbol{u}^{n+1}, \bar{\boldsymbol{u}}) - (p^{n+1}, \nabla\cdot\bar{\boldsymbol{u}}) \\ +2\,(\nu(c^{n+1})\boldsymbol{D}\boldsymbol{u}^{n+1}, \boldsymbol{D}\bar{\boldsymbol{u}}) = 0, \\ (\nabla\cdot\boldsymbol{u}^{n+1}, \bar{p}) = 0, \end{cases} \tag{3.17}$$

where $\widehat{\boldsymbol{u}} := \dfrac{\boldsymbol{u}^\star + \boldsymbol{u}^{\star\star}}{2}$.

Again, this scheme has the conservative property (3.12) and the local discrete energy law given by the following result.

Theorem 3.4
Schemes (3.15)–(3.17) satisfy the following local discrete energy law:

DOI: 10.1002/nme

$$\begin{aligned}\delta_t E(\boldsymbol{d}^{n+1}, c^{n+1}, \boldsymbol{u}^{n+1}) + \gamma_{nem}\,\|\boldsymbol{w}^{n+1}\|_{L^2}^2 + \gamma_{mix}\|\nabla\mu^{n+1}\|_{L^2}^2 + 2\,\|\nu(c^{n+1})^{1/2}\boldsymbol{D}\boldsymbol{u}^{n+1}\|_{L^2}^2 \\ + ND_{\boldsymbol{u}}^{n+1} + ND_{elast}^{n+1}(c^{n+1}) + ND_{penal}^{n+1}(c^{n+1}) + ND_{philic}^{n+1} \\ + ND_{phobic}^{n+1} + ND_{interp}^{n+1}(\boldsymbol{d}^n) + \overline{ND}_{anch}^{n+1} = 0,\end{aligned} \tag{3.18}$$

where $ND_{\boldsymbol{u}}^{n+1}, ND_{elast}^{n+1}(c^{n+1}), ND_{penal}^{n+1}(c^{n+1}), ND_{philic}^{n+1}, ND_{phobic}^{n+1}$, and $ND_{interp}^{n+1}(\boldsymbol{d}^n)$ are given in (3.14) and $\overline{ND}_{anch}^{n+1}$ is defined as

$$\begin{aligned}\overline{ND}_{anch}^{n+1} = \lambda_{anch}\,\frac{k}{2}\int_\Omega \delta_1\,\big[(|\boldsymbol{d}^n|^2|\delta_t\nabla c^{n+1}|^2 + |\delta_t\boldsymbol{d}^{n+1}|^2|\nabla c^{n+1}|^2) \\ +\delta_2\,\left(|\boldsymbol{d}^n\cdot\nabla\delta_t c^{n+1}|^2 + |\delta_t\boldsymbol{d}^{n+1}\cdot\nabla c^{n+1}|^2\right)\big]\,d\boldsymbol{x}.\end{aligned}$$

Again, the values of (δ_1, δ_2) depending on the type of anchoring were defined in (3.6).

Proof
The same arguments presented in the proof of Theorem 3.2 were followed. □

3.2. How to define $f_k(c^{n+1}, c^n)$, $\boldsymbol{g}_k(\boldsymbol{d}^{n+1}, \boldsymbol{d}^n)$, $i_k(c^{n+1}, c^n)$ to obtain linear unconditionally energy-stable schemes

There are many ways of handling the double-well potential term appearing in phase-field and nematic liquid crystal frameworks. Indeed, in the last years, a vast amount of literature has been devoted to derive new approximations, where each of these approximations has their own advantages and disadvantages. For a recent review on this topic, we refer the reader to [3].

We are interested in designing linear schemes; therefore, we need to consider a linear dependence of $f_k(c^{n+1}, c^n)$, $\boldsymbol{g}_k(\boldsymbol{d}^{n+1}, \boldsymbol{d}^n)$, and $i_k(c^{n+1}, c^n)$ with respect to the unknowns c^{n+1} and $\boldsymbol{d}^{n+1}$, such that the resulting scheme be energy stable. In this work, the key idea to define $f_k(c^{n+1}, c^n)$ and $\boldsymbol{g}_k(\boldsymbol{d}^{n+1}, \boldsymbol{d}^n)$ is to replace the original double-well potentials $F(c)$ and $G(\boldsymbol{d})$ by potentials $\tilde{F}(c)$ and $\tilde{G}(\boldsymbol{d})$, which coincide with $F(c)$ and $G(\boldsymbol{d})$ in the interval $[-1, 1]$ but are truncated otherwise by means of a quadratic growth, allowing us to control the numerical dissipation as was performed in [19]. Furthermore, the resulting way of designing the potential approximations can be naturally extended to $i_k(c^{n+1}, c^n)$ because $I(c)$ can be viewed as a truncated potential (see (2.4)). Without loss of generality, all the arguments considered to derive system (2.15) can be naturally extended by using potentials $\tilde{F}(c)$ and $\tilde{G}(\boldsymbol{d})$ instead of $F(c)$ and $G(\boldsymbol{d})$.

3.2.1. Potential $f_k(c^{n+1}, c^n)$. We change the potential $F(c)$ in (2.2) by a truncated version $\tilde{F}(c) \in C^2(\mathbb{R})$ with quadratic growth for $|c| > 1$, as follows:

$$\tilde{F}(c) = \begin{cases} \dfrac{1}{\varepsilon^2}(c+1)^2 & \text{if } c \leqslant -1\,, \\ \dfrac{1}{4\varepsilon^2}(c^2-1)^2 & \text{if } c \in [-1,1]\,, \\ \dfrac{1}{\varepsilon^2}(c-1)^2 & \text{if } c \geqslant 1\,. \end{cases} \tag{3.19}$$

Therefore, by differentiating,

$$\tilde{f}(c) = \begin{cases} \dfrac{2}{\varepsilon^2}(c+1) & \text{if } c \leqslant -1\,, \\ \dfrac{1}{\varepsilon^2}(c^2-1)\,c & \text{if } c \in [-1,1]\,, \\ \dfrac{2}{\varepsilon^2}(c-1) & \text{if } c \geqslant 1\,, \end{cases}$$

DOI: 10.1002/nme

and

$$\tilde{f}'(c) = \begin{cases} \dfrac{2}{\varepsilon^2} & \text{if } c \leqslant -1\,, \\ \dfrac{1}{\varepsilon^2}(3c^2-1) & \text{if } c \in [-1,1]\,, \\ \dfrac{2}{\varepsilon^2} & \text{if } c \geqslant 1\,. \end{cases} \tag{3.20}$$

Then, the proposed approximation of the potential term $f_k(c^{n+1}, c^n)$ reads

$$f_k(c^{n+1}, c^n) := \tilde{f}(c^n) + \frac{1}{2}\left\|\tilde{f}'\right\|_\infty (c^{n+1} - c^n)\,. \tag{3.21}$$

Notice that $f_k(c^{n+1}, c^n)$ is a first-order approximation of $f(c(t_{n+1}))$. In particular, taking into account the expression of $\tilde{f}'$ in (3.20), it is clear that $\|\tilde{f}'\|_\infty = \dfrac{2}{\varepsilon^2}$ and then (3.21) is written as

$$f_k(c^{n+1}, c^n) = \tilde{f}(c^n) + \frac{1}{\varepsilon^2}(c^{n+1} - c^n)\,. \tag{3.22}$$

Lemma 3.5
Let $\tilde{F} \in C^2(\mathbb{R})$ defined in (3.19) and $f_k(c^{n+1}, c^n)$ in (3.21). Then, the term ND^{n+1}_{phobic} given in (3.14) satisfies

$$ND^{n+1}_{phobic} \geqslant 0 \quad \forall\, n\,.$$

Proof
See Appendix. □

Remark 3.6
The choice in (3.22) does not coincide with the frequently considered concave–convex decomposition (e.g., [32, 33]),

$$f_k(c^{n+1}, c^n) = \tilde{f}_c(c^{n+1}) + \tilde{f}_e(c^n)\,, \tag{3.23}$$

based on the decomposition $\tilde{F}(c) = \tilde{F}_c(c) + \tilde{F}_e(c)$ with

$$\tilde{F}_c(c) := \frac{1}{\varepsilon^2}(c^2+1), \quad \tilde{F}_e(c) := \tilde{F}(c) - \tilde{F}_c(c) = \begin{cases} \dfrac{2}{\varepsilon^2}c & \text{if } c \leqslant -1\,, \\ \dfrac{1}{\varepsilon^2}\left(\dfrac{1}{4}c^4 - \dfrac{3}{2}c^2 - \dfrac{3}{4}\right) & \text{if } c \in [-1,1]\,, \\ -\dfrac{2}{\varepsilon^2}c & \text{if } c \geqslant 1\,, \end{cases}$$

and defining $\tilde{f}_c(c) = \tilde{F}_c'(c)$ and $\tilde{f}_e(c) = \tilde{F}_e'(c)$. In fact,

$$\tilde{f}_c(c) = \frac{2}{\varepsilon^2}\,c\,, \qquad \tilde{f}_e(c) = \begin{cases} \dfrac{2}{\varepsilon^2} & \text{if } c \leqslant -1\,, \\ \dfrac{1}{\varepsilon^2}(c^3 - 3c) & \text{if } c \in [-1,1]\,, \\ -\dfrac{2}{\varepsilon^2} & \text{if } c \geqslant 1\,. \end{cases}$$

DOI: 10.1002/nme

Observe that decomposition (3.23) can also be written as

$$f_k(c^{n+1}, c^n) = \tilde{f}(c^n) + \frac{2}{\varepsilon^2}\,(c^{n+1} - c^n)\,.$$

Therefore, comparing with (3.22) in this case, a higher numerical dissipation term is introduced $\left(\frac{2}{\varepsilon^2}\,(c^{n+1} - c^n)\right.$ instead of $\left.\frac{1}{\varepsilon^2}\,(c^{n+1} - c^n)\right)$.

3.2.2. Potential $i_k(c^{n+1}, c^n)$. We can just extend the ideas presented for the potential $f_k(c^{n+1}, c^n)$ to define $i_k(c^{n+1}, c^n)$, because the potential $I(c)$ defined in (2.4) is already a truncated potential and, in particular, it satisfies

$$i'(c) = \begin{cases} \dfrac{15}{4}\,(c^2 - 1)\,c & \text{if } c \in (-1, 1), \\ 0 & \text{in other case.} \end{cases} \tag{3.24}$$

Then, the proposed first-order approximation $i_k(c^{n+1}, c^n)$ of the potential term $i\,(c(t_{n+1}))$ reads

$$i_k(c^{n+1}, c^n) := i\,(c^n) + \frac{1}{2}\,\|i'\|_\infty\,(c^{n+1} - c^n)\,. \tag{3.25}$$

In particular, from (3.24), it is clear that $\|i'\|_\infty = (5\sqrt{3})/6$ and then

$$i_k(c^{n+1}, c^n) = i\,(c^n) + \frac{5\sqrt{3}}{12}\,(c^{n+1} - c^n)\,. \tag{3.26}$$

Lemma 3.7
Let $I \in C^2(\mathbb{R})$ defined in (2.4) and $i_k(c^{n+1}, c^n)$ in (3.25). Then, the term $ND^{n+1}_{interp}(\boldsymbol{d})$ given in (3.14) satisfies

$$ND^{n+1}_{interp}(\boldsymbol{d}) \geqslant 0 \quad \forall\, n\,.$$

Proof
The same arguments presented in the proof of Lemma 3.5 were followed. □

3.2.3. Potential $\boldsymbol{g}_k(\boldsymbol{d}^{n+1}, \boldsymbol{d}^n)$. We replace the definition of $G(\boldsymbol{d})$ given in (2.2) by a truncated version $\tilde{G}(\boldsymbol{d}) \in \mathcal{C}^2(\mathbb{R}^3)$ with quadratic growth if $|\boldsymbol{d}| > 1$, as follows:

$$\tilde{G}(\boldsymbol{d}) = \begin{cases} \dfrac{1}{\eta^2}(|\boldsymbol{d}| - 1)^2 & \text{if } |\boldsymbol{d}| \geqslant 1\,, \\ \dfrac{1}{4\eta^2}(|\boldsymbol{d}|^2 - 1)^2 & \text{if } |\boldsymbol{d}| \leqslant 1\,. \end{cases} \tag{3.27}$$

Therefore, its first derivative is

$$\tilde{\boldsymbol{g}}(\boldsymbol{d}) = \begin{cases} \dfrac{2}{\eta^2}\,(|\boldsymbol{d}| - 1)\,\dfrac{\boldsymbol{d}}{|\boldsymbol{d}|} & \text{if } |\boldsymbol{d}| \geqslant 1\,, \\ \dfrac{1}{\eta^2}(|\boldsymbol{d}|^2 - 1)\,\boldsymbol{d} & \text{if } |\boldsymbol{d}| \leqslant 1\,, \end{cases}$$

and the Hessian matrix is

$$H_{\boldsymbol{d}}\tilde{G}_{ij}(\boldsymbol{d}) = \begin{cases} \dfrac{1}{\eta^2}\left(\dfrac{2}{|\boldsymbol{d}|^3}\,\boldsymbol{d}_i\,\boldsymbol{d}_j + 2\,\dfrac{(|\boldsymbol{d}| - 1)}{|\boldsymbol{d}|}\,\delta_{ij}\right) & \text{if } |\boldsymbol{d}| \geqslant 1\,, \\ \dfrac{1}{\eta^2}\left(2\,\boldsymbol{d}_i\,\boldsymbol{d}_j + \left(|\boldsymbol{d}|^2 - 1\right)\,\delta_{ij}\right) & \text{if } |\boldsymbol{d}| \leqslant 1\,. \end{cases}$$

DOI: 10.1002/nme

Then, the proposed first-order approximation $\boldsymbol{g}_k(\boldsymbol{d}^{n+1}, \boldsymbol{d}^n)$ of the potential term $\boldsymbol{g}(\boldsymbol{d}(t_{n+1}))$ reads

$$\boldsymbol{g}_k(\boldsymbol{d}^{n+1}, \boldsymbol{d}^n) = \tilde{\boldsymbol{g}}(\boldsymbol{d}^n) + \frac{1}{2}\|\tilde{\boldsymbol{g}}'\|_\infty (\boldsymbol{d}^{n+1} - \boldsymbol{d}^n). \tag{3.28}$$

Lemma 3.8
Let $\tilde{G} \in C^2(\mathbb{R}^3)$ defined in (3.27) and $\boldsymbol{g}_k(\boldsymbol{d}^{n+1}, \boldsymbol{d}^n)$ in (3.28). It holds

$$ND^{n+1}_{penal}(c) \geqslant 0 \quad \forall\, n\,.$$

Proof
See Appendix. □

Now, we are in position to state the following energy-stability result.

Theorem 3.9
Schemes (3.3)–(3.11) and (3.15)–(3.17) using the potential approximations (3.22), (3.26), and (3.28) are linear and unconditionally energy stable (see Definition (3.1)).

Proof
The linearity of both schemes is trivial. We are going to assure the energy stability of the schemes, because all the numerical dissipation terms will be positive or zero. By definition, it is clear that

$$ND^{n+1}_{\boldsymbol{u}} \geqslant 0\,, \quad ND^{n+1}_{elast}(c^n) \geqslant 0\,, \quad ND^{n+1}_{elast}(c^{n+1}) \geqslant 0\,, \quad \text{and} \quad ND^{n+1}_{philic} \geqslant 0\,.$$

Moreover, by Lemmas 3.5, 3.7, and 3.8, it is clear that

$$ND^{n+1}_{penal}(c^n) \geqslant 0\,, \quad ND^{n+1}_{penal}(c^{n+1}) \geqslant 0\,, \quad ND^{n+1}_{phobic} \geqslant 0\,, \quad \text{and} \quad ND^{n+1}_{interp}(\boldsymbol{d}) \geqslant 0\,.$$

Finally, taking into account the relation $|a|^2|b|^2 - |a \cdot b|^2 \geqslant 0$, it is easy to show

$$ND^{n+1}_{anch} \geqslant 0 \quad \text{and} \quad \overline{ND}^{n+1}_{anch} \geqslant 0\,.$$

□

Remark 3.10
Adding the local in time discrete energy law (3.1), it is possible to obtain the global estimates (2.17), (2.18), and (2.21) following the same argument carried out at the end of Section 2. In particular, in order to derive the estimate like (2.21) for $(\boldsymbol{d}^n)$ in the whole domain, we have to impose the constraint $\boldsymbol{D}_h \subseteq \boldsymbol{W}_h$ and to use the discrete Gronwall's lemma.

3.3. Well-posedness of the schemes

We study the well-posedness of all the sub-steps of the c-$\boldsymbol{d}$-$\boldsymbol{u}$ scheme (the corresponding proofs for the $\boldsymbol{d}$-c-$\boldsymbol{u}$ scheme can be derived just following the same arguments).

Lemma 3.11
If $1 \in C_h$, then there exist a unique solution (c^{n+1}, μ^{n+1}) of (3.15) using the potential approximations (3.22) and (3.26) for $f_k(c^{n+1}, c^n)$ and $i_k(c^{n+1}, c^n)$, respectively.

Proof
See Appendix. □

Lemma 3.12
If $\boldsymbol{D}_h \subseteq \boldsymbol{W}_h$, then there exist a unique solution $(\boldsymbol{d}^{n+1}, \boldsymbol{w}^{n+1})$ of (3.16) using the potential approximation (3.28) for $\boldsymbol{g}_k(\boldsymbol{d}^{n+1}, \boldsymbol{d}^n)$.

DOI: 10.1002/nme

Proof
See Appendix. □

Lemma 3.13
If the pair of finite element spaces $(\boldsymbol{V}_h, P_h)$ satisfies the discrete *inf-sup* condition

$$\exists\, \beta > 0 \quad \text{such that} \quad \|p\|_{L^2} \leqslant \beta \sup_{\bar{\boldsymbol{u}} \in V_h \setminus \{\Theta\}} \frac{(p, \nabla \cdot \bar{\boldsymbol{u}})}{\|\bar{\boldsymbol{u}}\|_{H^1}} \quad \forall\, p \in P_h\,, \tag{3.29}$$

then there exist a unique solution $(\boldsymbol{u}^{n+1}, p^{n+1})$ of (3.17).

Proof
See Appendix. □

3.4. Some possibilities for discrete spaces

We now specify some examples of finite element subspaces to approximate our numerical scheme.

- In order to obtain $O(h^2)$ accuracy for the unknowns $(\boldsymbol{u}, p, \boldsymbol{d}, \boldsymbol{w}, c, \mu) \in \boldsymbol{H}^1(\Omega) \times L^2(\Omega) \times \boldsymbol{H}^1(\Omega) \times \boldsymbol{L}^2(\Omega) \times H^1(\Omega) \times H^1(\Omega)$, the natural choice is

$$(\boldsymbol{u}, p) \sim P_2 \times P_1\,, \qquad (c, \mu) \sim P_2 \times P_2\,, \qquad \text{and} \qquad (\boldsymbol{d}, \boldsymbol{w}) \sim P_2 \times P_1\,. \tag{3.30}$$

  The problem of this approach is that the constraint $\boldsymbol{D}_h \subseteq \boldsymbol{W}_h$ does not hold.
- In order to obtain $O(h)$ accuracy for the unknowns $(\boldsymbol{u}, p, \boldsymbol{d}, \boldsymbol{w}, c, \mu) \in \boldsymbol{H}^1(\Omega) \times L^2(\Omega) \times \boldsymbol{H}^1(\Omega) \times \boldsymbol{L}^2(\Omega) \times H^1(\Omega) \times H^1(\Omega)$, the natural choice is

$$(\boldsymbol{u}, p) \sim P_1 \times P_0\,, \qquad (c, \mu) \sim P_1 \times P_1\,, \qquad \text{and} \qquad (\boldsymbol{d}, \boldsymbol{w}) \sim P_1 \times P_0\,. \tag{3.31}$$

  The problems of this approach are that the constraint $\boldsymbol{D}_h \subseteq \boldsymbol{W}_h$ does not hold and the spaces for the velocity–pressure pair does not satisfy the discrete *inf-sup* condition (3.29).
- We propose the following choice for the discrete spaces:

$$(\boldsymbol{u}, p) \sim P_2 \times P_1\,, \qquad (c, \mu) \sim P_1 \times P_1\,, \qquad \text{and} \qquad (\boldsymbol{d}, \boldsymbol{w}) \sim P_1 \times P_1\,, \tag{3.32}$$

  which have $O(h)$ accuracy and satisfy the assumptions of Lemmas 3.11, 3.12, and 3.13.

4. NUMERICAL SIMULATIONS

In this section, we present numerical experiments to show the effectiveness of the numerical schemes and the approximation of the potentials derived in the paper. In particular, we have considered the c-$\boldsymbol{d}$-$\boldsymbol{u}$ scheme presented in Section 3.1.4, where the potential terms have been approximated considering the ideas introduced in Section 3.2. All the simulations have been carried out in two dimensions using FREEFEM++ software [34], and we consider the choice for the discrete spaces presented in (3.32). The discrete and physical parameters are presented in Table I, where for simplicity we are considering constant viscosity $\nu(c) = \nu_0$.

Moreover, the boundary conditions considered in all the simulations are

$$\boldsymbol{u}|_{\partial\Omega} = (I(c)\nabla \boldsymbol{d})\boldsymbol{n}|_{\partial\Omega} = \boldsymbol{0}, \quad \left.\frac{\partial c}{\partial \boldsymbol{n}}\right|_{\partial\Omega} = \left.\frac{\partial \mu}{\partial \boldsymbol{n}}\right|_{\partial\Omega} = 0\,, \tag{4.1}$$

Table I. Parameters.

Ω	$[0,T]$	h	dt	ν_0	λ_{nem}	λ_{mix}	λ_{anch}	γ_{nem}	γ_{mix}	ε	η
$[-1,1]^2$	$[0,10]$	$2/90$	0.001	1.0	0.1	0.01	0.1	0.5	0.01	0.05	0.075

DOI: 10.1002/nme

and the velocity is initially set to zero ($\boldsymbol{u} = 0$) in all the cases. For all the simulations, we present the evolution in time of the total energies jointly with the dynamic of the phase-field function c and the director vector $\boldsymbol{d}$. In the figures, we have omitted the velocity field $\boldsymbol{u}$, because our experiments have been designed such that the kinetic energy is not playing a main role in the behavior of the system, in order to be able to identify the influence of the rest of the terms.

We are interested in how the competition between the different energies involved in the definition of the total energy (2.1) (i.e., the competition between the different processes) influences the behavior of the system. To this end, we have compared the behavior of the three possible choices of the anchoring energy (no anchoring, parallel, and homeotropic) in three different settings. In the first experiment, we focus on the equilibrium configurations that can be obtained with homogeneous director vector fields, while in the second and third cases, the initial condition has been designed combining ideas from numerical experiments for phase-field models and for nematic liquid crystals.

4.1. Experiment 1. Circular droplet of nematic liquid crystal without defects in an isotropic fluid

We consider the spatial domain $[-1, 1] \times [-1, 1]$ and the time interval $[0, 10]$. In the first one, we consider a circular droplet of nematic liquid crystal in an isotropic fluid filling the domain, where initially the director vector $\boldsymbol{d}$ is parallel to the y-axis. In this case, we observe how the dynamic is completely different depending on the type of anchoring. In Figure 3, we plot the results obtained for no anchoring, parallel, and homeotropic anchoring, respectively. It is clear how the anchoring energy influences the dynamic of the system, arriving at completely different equilibrium configurations, while in all the cases, the total energy of the system is decreasing until it reaches an equilibrium state (Figure 4).

4.2. Experiment 2. Circular droplet of nematic liquid crystal with defects in an isotropic fluid

In the second experiment, instead of a circular shape filled with a uniform director vector, we have considered an elliptic nematic droplet with two defect points at $(\pm 1/2, 0)$, a Hedgehog defect at $(1/2, 0)$ and an anti-Hedgehog defect at $(-1/2, 0)$. This initial configuration for $\boldsymbol{d}$ has been widely used in the literature related to numerical approximation of nematic liquid crystals (we refer to Reference [3] for a review and related references on this topic) and is generated by using the function

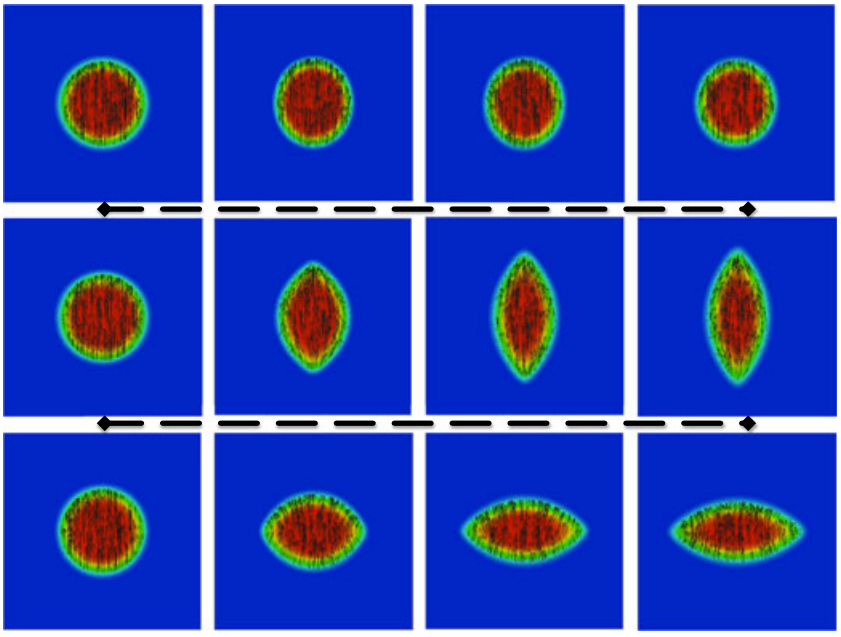

Figure 3. Experiment 1. Dynamic of phase-field function c and director vector field $\boldsymbol{d}$ at time $t = 0.0, 1.0, 5.0, 10.0$. First row, no anchoring; second row, parallel; and third row, homeotropic.

DOI: 10.1002/nme

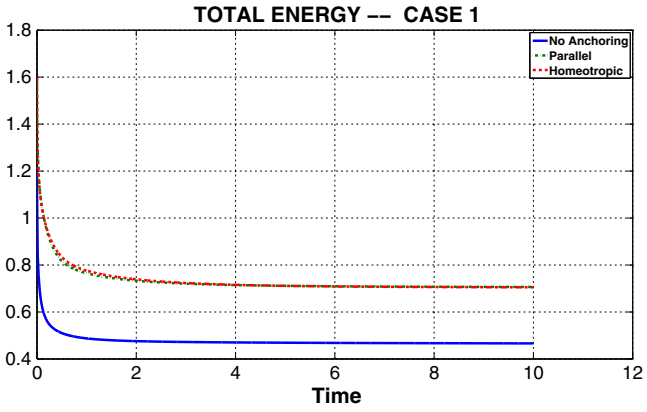

Figure 4. Experiment 1. Total energy for the parallel, homeotropic, and no anchoring.

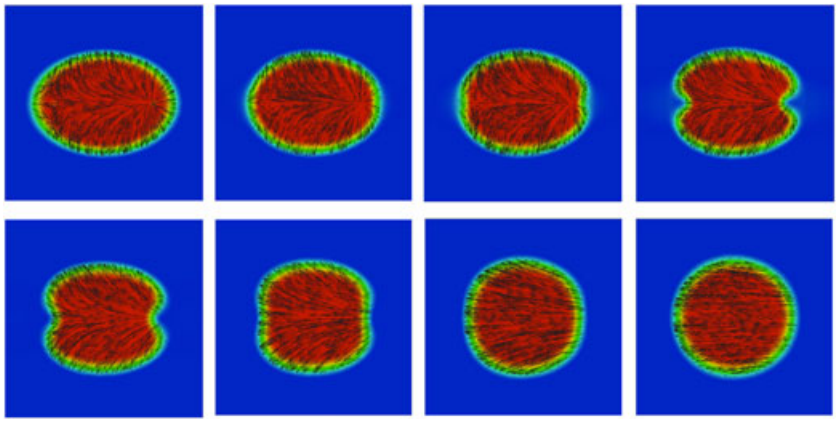

Figure 5. Experiment 2. No anchoring: (from left to right and up to down) dynamic of phase field c and director vector $\boldsymbol{d}$ at time $t = 0.0, 0.3, 0.5, 1.0, 1.5, 2.5, 5.0, 10.0$.

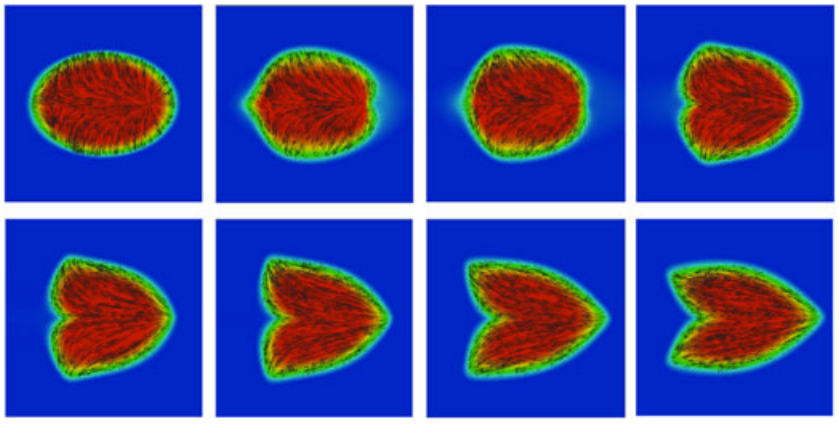

Figure 6. Experiment 2. Parallel anchoring: (from left to right and up to down) dynamic of phase field c and director vector $\boldsymbol{d}$ at time $t = 0.0, 0.3, 0.5, 1.0, 1.5, 2.5, 5.0, 10.0$.

$$\boldsymbol{d}_0(x) = I(c)\,\widehat{\boldsymbol{d}}/\sqrt{|\widehat{\boldsymbol{d}}|^2 + 0.05^2}, \quad \text{with} \quad \widehat{\boldsymbol{d}} = (x^2 + y^2 - 0.25, y)\,. \tag{4.2}$$

In this case, there are three main processes that are competing: In order to minimize the mixing energy, the system should arrive to a circular configuration, while to minimize the elastic energy, the

DOI: 10.1002/nme

system should annihilate the defects. Finally, to minimize the anchoring energy, the system should arrive to the equilibrium states observed in the three cases considered in Figure 3.

The results obtained are presented in Figures 5, 6, and 7. Moreover, we plot the evolution of the total energy of each case in Figure 8. It is interesting to see how the evolution of the three cases

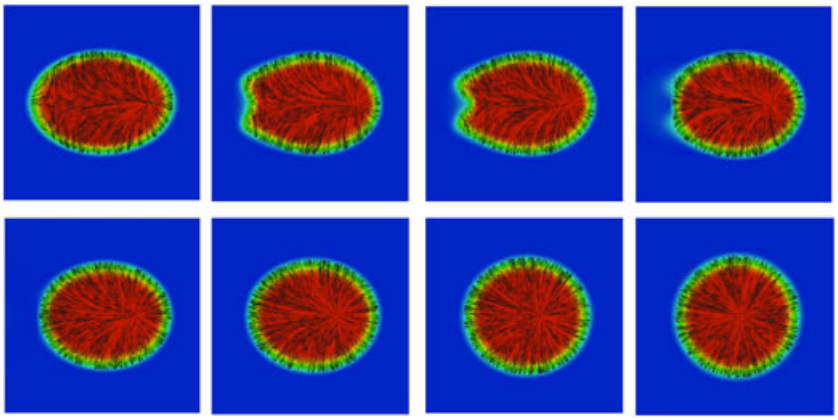

Figure 7. Experiment 2. Homeotropic anchoring: (from left to right and up to down) dynamic of phase field c and director vector $\boldsymbol{d}$ at time $t = 0.0, 0.3, 0.5, 1.0, 1.5, 2.5, 5.0, 10.0$.

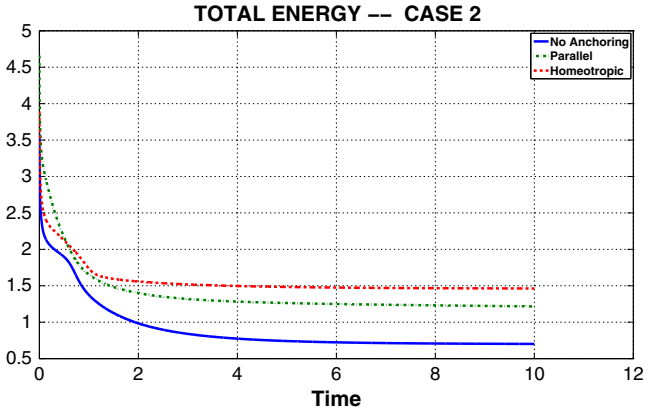

Figure 8. Experiment 2. Total energy for the parallel, homeotropic, and no anchoring.

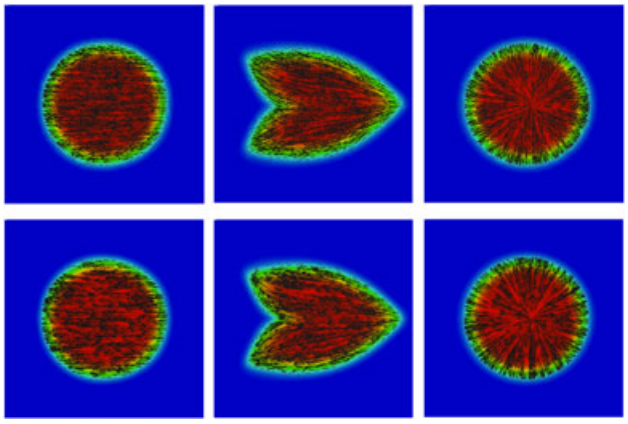

Figure 9. Comparison of the equilibrium configurations using different meshes. First row, 60×60; second row, 120×120. Phase field c and director vector $\boldsymbol{d}$ at time $t = 10.0$ for no anchoring, parallel, and homeotropic (from left to right).

DOI: 10.1002/nme

is completely different. When no anchoring energy is considered (Figure 5), the system annihilates the defects in a symmetric way, arriving at an equilibrium state formed by a circular-shaped droplet with a uniform director vector $\boldsymbol{d}$ parallel to the x-axis. If the anchoring energy is not zero, we observe different dynamics. On one hand, the parallel anchoring (Figure 6) enforces a constraint to the director vector on the interface that plays an important role on the way of how the defects are annihilated, and we observe how the system is evolving to an equilibrium state that is different to the observed in the first experiment (Figure 3). On the other hand, the choice of the homeotropic anchoring (Figure 7) also imposes a constraint on the possible behavior of the director vector on the interface, and in this case, it is not feasible to annihilate both defects. As a result, instead of the configuration obtained in the first experiment, the equilibrium state corresponds to a circular nematic droplet with a defect in the center.

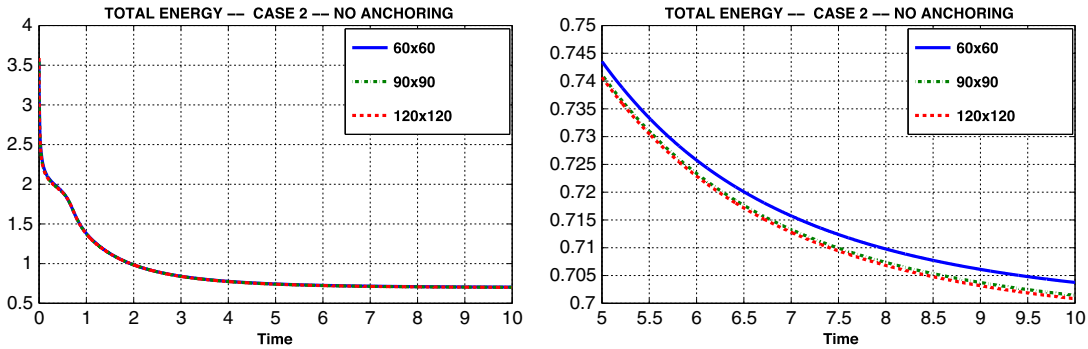

Figure 10. (From left to right) Comparison of the total energy using different meshes for the no anchoring case in the interval $t \in [0, 10]$ and a zoom at $t \in [5, 10]$.

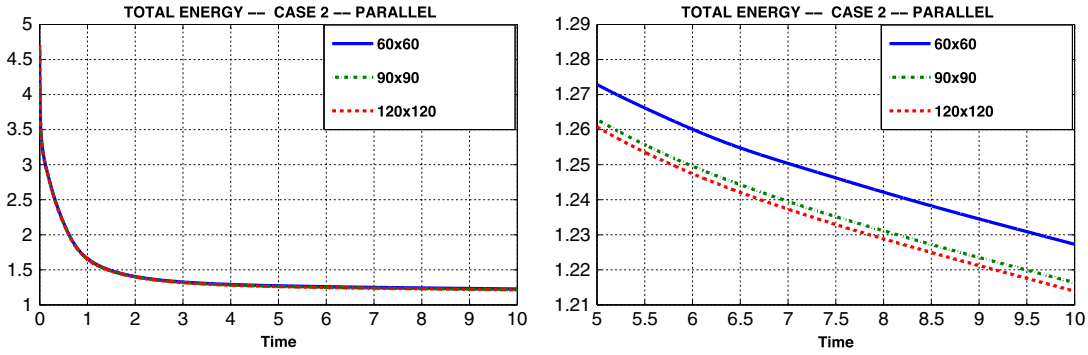

Figure 11. (From left to right) Comparison of the total energy using different meshes for the parallel case in the interval $t \in [0, 10]$ and a zoom at $t \in [5, 10]$.

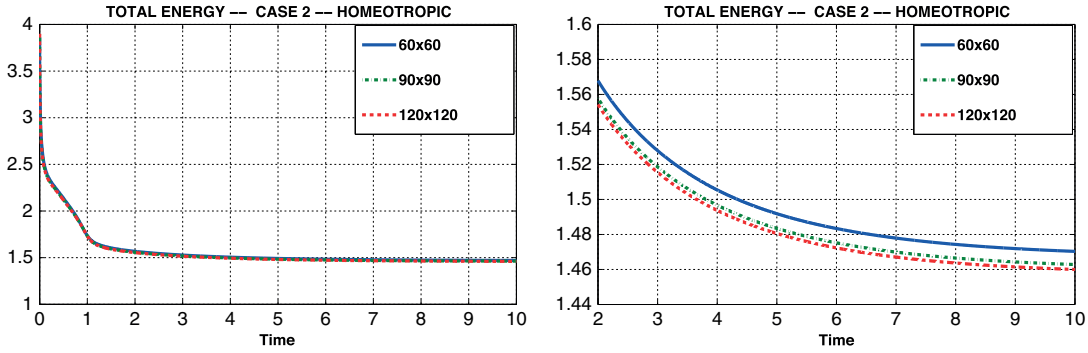

Figure 12. (From left to right) Comparison of the total energy using different meshes for the homeotropic case in the interval $t \in [0, 10]$ and a zoom at $t \in [2, 10]$.

DOI: 10.1002/nme

4.2.1. Stability and computational cost of the results. In order to study the stability of the computed results, we have carried out the simulations using different meshes. In particular, we have compared the results using the same parameters of Section 4.2 with a coarser (60×60) and a finer mesh (120×120). The equilibrium configurations are shown in Figure 9, and the comparison of the total energy in each case is presented in Figures 10, 11, and 12. In all the cases, we obtain the same dynamics, and as expected, there is numerical convergence when the mesh is refined.

Moreover, we have compared the previous results with a linearized version of the coupled scheme (3.2) using the coarser mesh (60×60). We obtain the same dynamics in both cases (Figures 13–16), but the computational cost for the coupled scheme is much higher than for the splitting one. In this case, using a 60×60 mesh in a computer with 2×2.26 GHz Quad-Core Intel Xeon with

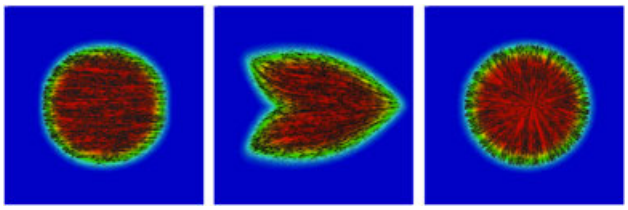

Figure 13. Equilibrium configurations using a linearized coupled numerical scheme for a 60×60 mesh. Phase field c and director vector $\boldsymbol{d}$ at time $t = 10.0$ for no anchoring, parallel, and homeotropic (from left to right).

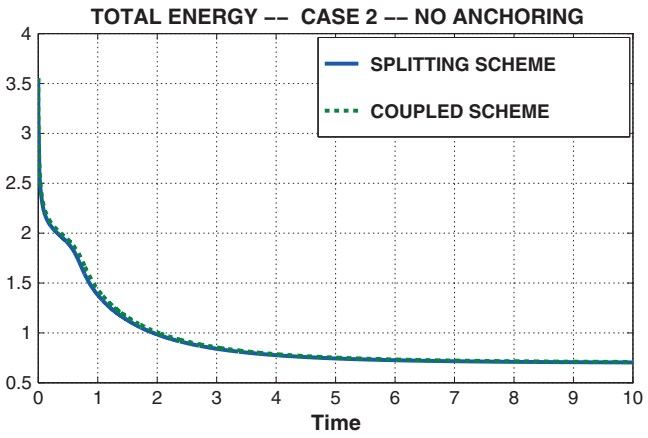

Figure 14. Comparison of the total energy between coupled and splitting scheme for the no anchoring case.

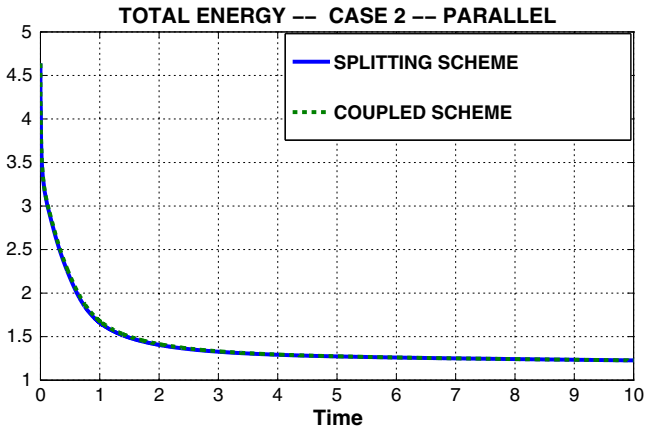

Figure 15. Comparison of the total energy between coupled and splitting scheme for the parallel case.

DOI: 10.1002/nme

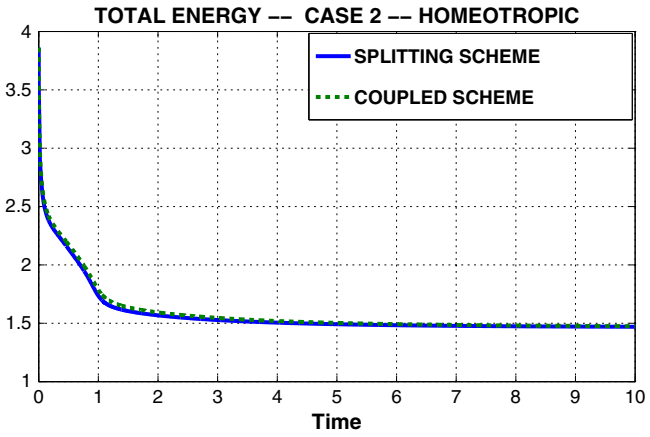

Figure 16. Comparison of the total energy between coupled and splitting scheme for the homeotropic case.

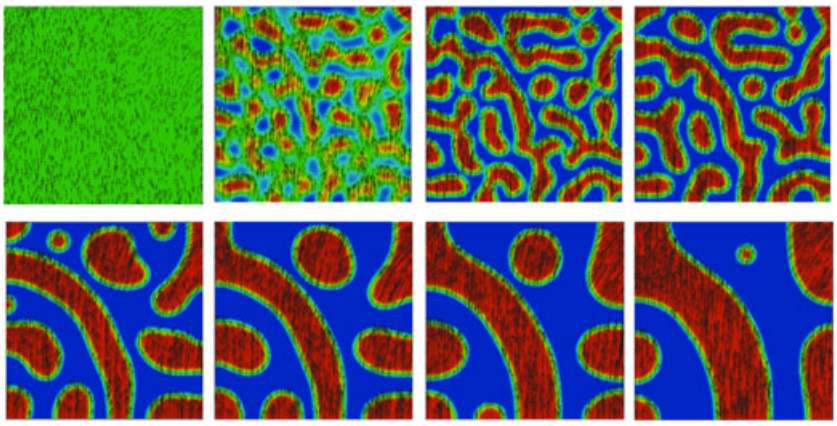

Figure 17. Experiment 3. No anchoring: (from left to right and up to down) dynamic of phase field c and director vector $\boldsymbol{d}$ at time $t = 0.0, 0.02, 0.03, 0.05, 0.15, 0.25, 0.5, 1.0$.

12 Gb 1066 MHz DDR3, each iteration takes around 36 s for the coupled scheme and around 8 s for the splitting scheme (computing the three sub-steps); that is, in this case, the splitting scheme is 4.5 times faster than the coupled one. In the case of considering a 90×90 mesh, one iteration of the coupled scheme takes 83 s, while the splitting one takes 19 s; that is, in this case, the splitting scheme is 4.36 times faster than the coupled one.

4.3. Experiment 3. Spinodal decomposition

In the third experiment, we study the pattern formation produced by considering as initial condition for the three types of anchoring the same random initial data for the phase-field variable c, taking values between -10^{-2} and 10^{-2}, in order to simulate a spinodal decomposition. In this case, we consider the spatial domain $[0, 1] \times [0, 1]$ and the time interval $[0, 1]$. The initial director vector is computed using the following function:

$$\boldsymbol{d} = I(c)\ (\sin(x\,y)\sin(x\,y), \cos(x\,y)\cos(x\,y))\ .$$

It can be observed in Figure 17 how the case of not considering anchoring does not produce any regular pattern in the dynamics of the system. On the contrary, it is clear from Figure 18 that the parallel anchoring induces the system to create vertical stripes (parallel to the y-axis) in order to create interfaces that are parallel to the initial orientation vector, as the director vector also aligns vertically. As it can be observed in Figure 19, by considering homeotropic anchoring, we obtain something equivalent but with horizontal stripes (parallel to the x-axis) in order to create interfaces

DOI: 10.1002/nme

that are orthogonal to the director vector. Finally, in Figure 20, we plot the evolution of the total energy of each case, showing that in all cases, the total energy of the system is decreasing in time in order to arrive at an equilibrium configuration.

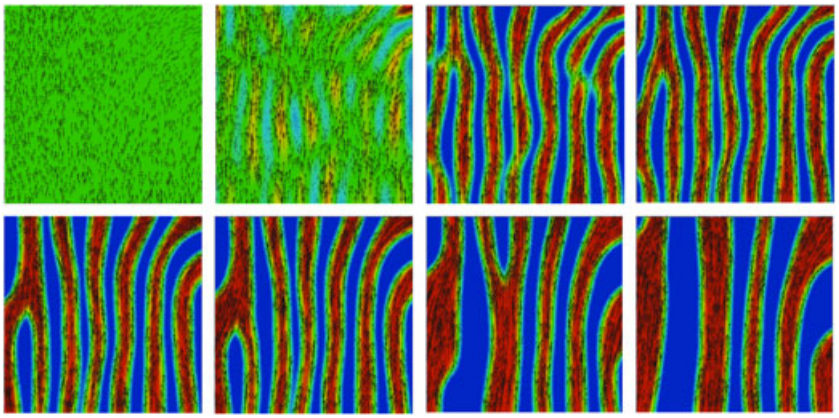

Figure 18. Experiment 3. Parallel anchoring: (from left to right and up to down) dynamic of phase field c and director vector $\boldsymbol{d}$ at time $t = 0.0, 0.02, 0.03, 0.05, 0.15, 0.25, 0.5, 1.0$.

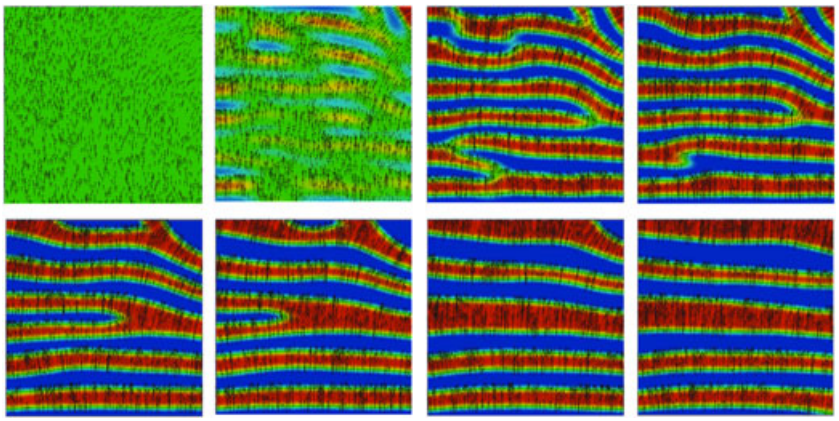

Figure 19. Experiment 3. Homeotropic anchoring: (from left to right and up to down) dynamic of phase field c and director vector $\boldsymbol{d}$ at time $t = 0.0, 0.02, 0.03, 0.05, 0.15, 0.25, 0.5, 1.0$.

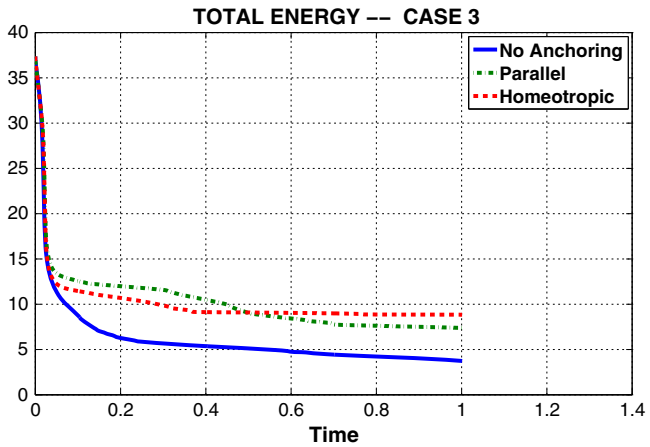

Figure 20. Experiment 3. Total energy for the parallel, homeotropic, and no anchoring.

DOI: 10.1002/nme

5. CONCLUSIONS

In this paper, we have studied the complex fluid mixture between isotropic (Newtonian fluid) and nematic flows, taking into account viscous, mixing, nematic, and anchoring effects. Firstly, we have introduced a new differential problem to model nematic–isotropic mixtures, reformulating the stress tensors in order to design an efficient numerical approximation. Then, we have derived two new linear splitting schemes that allow us to decouple the computation of the three pairs of unknowns $(\boldsymbol{v}, p)$ (velocity–pressure), (c, μ) (phase field–chemical potential), and $(\boldsymbol{d}, \boldsymbol{w})$ (director vector–equilibrium). Moreover, we have proven that these formulations are unconditionally energy stable, because they satisfy a discrete energy law independently of the size of the space and time meshes considered. The fact of being able to decouple the computations in different linear sub-steps maintaining the discrete energy law is crucial to carry out relevant numerical experiments under a feasible computational cost and assuring the accuracy of the computed results.

Several numerical computations using these new numerical schemes have been reported, showing the good performance of the proposed method considering different initial conditions. In all the cases, the energy stability is numerically achieved, and we illustrate how the anchoring effects characterize the behavior of the system, arriving at equilibrium configurations that have been already predicted by experimental groups [9, 10].

Finally, there are several interesting open questions that we plan to address in our future research: comparison of the numerical schemes with realistic experimental settings, derivation of second-order-in-time splitting schemes, study of the numerical order of convergence of the proposed numerical scheme, and implementation of three-dimensional numerical simulations.

APPENDIX

Proof of Lemma 2.3

From the contribution of the mixture process to the stress σ_{mix} given in (2.11) together with the definition of μ given in (2.8), we deduce the following:

$$\begin{aligned} -\nabla\cdot\sigma_{mix} &= \lambda_{mix}\left(\nabla c\,\Delta c + \frac{1}{2}\nabla|\nabla c|^2\right) \\ &= -\lambda_{mix}[-\Delta c + F'(c)]\nabla c + \lambda_{mix}\nabla\left(\frac{1}{2}|\nabla c|^2 + F(c)\right) \\ &= -\mu\,\nabla c + \lambda_{nem} I'(c)\left(\frac{1}{2}|\nabla \boldsymbol{d}|^2 + G(\boldsymbol{d})\right)\nabla c + \lambda_{anch}\frac{\delta E_{anch}}{\delta c}\nabla c \\ &\quad + \lambda_{mix}\nabla\left(\frac{1}{2}|\nabla c|^2 + F(c)\right). \end{aligned} \tag{A.1}$$

On the other hand, using the definition of $\boldsymbol{w}$ given in (2.7) in the contribution of the nematic part to the stress σ_{nem}, we have

$$\begin{aligned} -\nabla\cdot\sigma_{nem} &= \lambda_{nem}\left((\nabla\boldsymbol{d})^t\nabla\cdot(I(c)\nabla\boldsymbol{d}) + I(c)\frac{1}{2}\nabla|\nabla\boldsymbol{d}|^2\right) \\ &= -\lambda_{nem}\left[(\nabla\boldsymbol{d})^t[-\nabla\cdot(I(c)\nabla\boldsymbol{d}) + I(c)\,G'(\boldsymbol{d})] - I(c)\nabla\left(\frac{1}{2}|\nabla\boldsymbol{d}|^2 + G(\boldsymbol{d})\right)\right] \\ &= -(\nabla\boldsymbol{d})^t\boldsymbol{w} + \lambda_{anch}\,(\nabla\boldsymbol{d})^t\frac{\delta E_{anch}}{\delta\boldsymbol{d}} + \lambda_{nem}\nabla\left[I(c)\left(\frac{1}{2}|\nabla\boldsymbol{d}|^2 + G(\boldsymbol{d})\right)\right] \\ &\quad - \lambda_{nem} I'(c)\left(\frac{1}{2}|\nabla\boldsymbol{d}|^2 + G(\boldsymbol{d})\right)\nabla c. \end{aligned} \tag{A.2}$$

DOI: 10.1002/nme

Moreover, for the anchoring contribution σ_{anch}, we detail the calculations in the homeotropic anchoring case (the parallel case can be treated in an analogous way). Taking first derivatives of σ_{anch}, we have

$$\begin{aligned}-\partial_j(\sigma_{anch})_{ij} &= -\lambda_{anch}\,\partial_j\left[(\boldsymbol{d}\cdot\nabla c)\;\boldsymbol{d}_j\,\partial_i c - |\boldsymbol{d}|^2\,\partial_i c\,\partial_j c\right]\\ &= -\lambda_{anch}\,\left(\partial_j\left[(\boldsymbol{d}\cdot\nabla c)\,\boldsymbol{d}_j - |\boldsymbol{d}|^2\,\partial_j c\right]\,\partial_i c + (\boldsymbol{d}\cdot\nabla c)\,\boldsymbol{d}_j\,\partial^2_{ij}c - |\boldsymbol{d}|^2\,\partial_j c\,\partial^2_{ij}c\right)\,.\end{aligned}$$

Then, combining the previous expression with the following relations

$$\partial_i\left(\boldsymbol{d}_j\,\partial_j c\right) = \partial_i\boldsymbol{d}_j\,\partial_j c + \boldsymbol{d}_j\,\partial^2_{ij}c\,,$$

and

$$|\boldsymbol{d}|^2\,\partial_i(|\nabla c|^2) = \partial_i\left(|\boldsymbol{d}|^2\,|\nabla c|^2\right) - 2\,|\nabla c|^2\,\boldsymbol{d}\cdot\partial_i\boldsymbol{d}\,,$$

and taking into account relations (2.9), (2.10), and (2.14), we can arrive at

$$\begin{aligned}-\nabla\cdot\sigma_{anch} &= -\lambda_{anch}\,\Big[\nabla\cdot\left[(\boldsymbol{d}\cdot\nabla c)\,\boldsymbol{d} - |\boldsymbol{d}|^2\,\nabla c\right]\,\nabla c\\ &\qquad + (\nabla\boldsymbol{d})^t\left(|\nabla c|^2\boldsymbol{d} - (\boldsymbol{d}\cdot\nabla c)\,\nabla c\right) + \frac{1}{2}\,\nabla\left(|\boldsymbol{d}\cdot\nabla c|^2 - |\boldsymbol{d}|^2\,|\nabla c|^2\right)\Big]\\ &= -\lambda_{anch}\,\left((\nabla\boldsymbol{d})^t\,\frac{\delta E_{anch}}{\delta\boldsymbol{d}} + \frac{\delta E_{anch}}{\delta c}\nabla c\right) + \frac{\lambda_{anch}}{2}\nabla(W(\boldsymbol{d},c)).\end{aligned} \tag{A.3}$$

Note that using the same arguments, in the parallel anchoring case, it is possible to deduce

$$\begin{aligned}-\nabla\cdot\sigma_{anch} &= -\lambda_{anch}\,\left[(\boldsymbol{d}\cdot\nabla c)\,(\nabla\boldsymbol{d})^t\nabla c - \nabla\cdot((\boldsymbol{d}\cdot\nabla c)\,\boldsymbol{d})\,\nabla c - \frac{1}{2}\,\nabla\left(|\boldsymbol{d}\cdot\nabla c|^2\right)\right]\\ &= -\lambda_{anch}\,\left((\nabla\boldsymbol{d})^t\,\frac{\delta E_{anch}}{\delta\boldsymbol{d}} + \frac{\delta E_{anch}}{\delta c}\nabla c\right) + \frac{\lambda_{anch}}{2}\nabla(W(\boldsymbol{d},c)).\end{aligned} \tag{A.4}$$

Finally, adding up expressions (A.1), (A.2), and (A.3) or (A.4) , we arrive at (2.13). □

Proof of Theorem 3.2

For the sake of simplicity, we will only show the case of homeotropic anchoring. Indeed, the parallel anchoring case can be studied using the same arguments, while the no anchoring case is just a trivial generalization.

Taking $(\bar{\boldsymbol{w}},\bar{\boldsymbol{d}}) = (\boldsymbol{w}^{n+1},\delta_t\boldsymbol{d}^{n+1})$ in (3.3), we obtain

$$\begin{aligned}&\gamma_{nem}\,\|\boldsymbol{w}^{n+1}\|^2_{L^2} + ND^{n+1}_{elast}(c^n) + ND^{n+1}_{penal}(c^n)\\ &\qquad + \lambda_{nem}\int_\Omega I(c^n)\,\delta_t\left(\frac{|\nabla\boldsymbol{d}^{n+1}|^2}{2} + G(\boldsymbol{d}^{n+1})\right)d\boldsymbol{x}\\ &\qquad + \frac{\lambda_{anch}}{2k}\,\delta_1\int_\Omega\left[|\nabla c^n|^2|\boldsymbol{d}^{n+1}|^2 - |\nabla c^n|^2|\boldsymbol{d}^n|^2 + |\nabla c^n|^2|\boldsymbol{d}^{n+1}-\boldsymbol{d}^n|^2\right]d\boldsymbol{x}\\ &\qquad + \frac{\lambda_{anch}}{2k}\,\delta_2\int_\Omega\left[|\boldsymbol{d}^{n+1}\cdot\nabla c^n|^2 - |\boldsymbol{d}^n\cdot\nabla c^n|^2 + |(\boldsymbol{d}^{n+1}-\boldsymbol{d}^n)\cdot\nabla c^n|^2\right]d\boldsymbol{x}\\ &\qquad = -\left((\boldsymbol{u}^\star\cdot\nabla)\boldsymbol{d}^n,\boldsymbol{w}^{n+1}\right).\end{aligned} \tag{A.5}$$

DOI: 10.1002/nme

On the other hand, taking $(\bar{\mu}, \bar{c}) = (\mu^{n+1}, \delta_t c^{n+1})$ in (3.7), we obtain

$$\begin{aligned}
&\gamma_{mix}\|\nabla\mu^{n+1}\|_{L^2}^2 + ND_{philic}^{n+1} + ND_{phobic}^{n+1} + ND_{interp}^{n+1} \\
&+\lambda_{mix}\,\delta_t E_{mix}(c^{n+1}) \\
&+\lambda_{nem}\int_\Omega \left(\frac{|\nabla \boldsymbol{d}^{n+1}|^2}{2} + G(\boldsymbol{d}^{n+1})\right)\delta_t I(c^{n+1})d\boldsymbol{x} \\
&+\frac{\lambda_{anch}}{2k}\,\delta_1\int_\Omega \left[|\nabla c^{n+1}|^2|\boldsymbol{d}^{n+1}|^2 - |\nabla c^n|^2|\boldsymbol{d}^{n+1}|^2 + |\nabla(c^{n+1}-c^n)|^2|\boldsymbol{d}^{n+1}|^2\right]d\boldsymbol{x} \\
&+\frac{\lambda_{anch}}{2k}\,\delta_2\int_\Omega \left[|\boldsymbol{d}^{n+1}\cdot\nabla c^{n+1}|^2 - |\boldsymbol{d}^{n+1}\cdot\nabla c^n|^2 + |\boldsymbol{d}^{n+1}\cdot\nabla(c^{n+1}-c^n)|^2\right]d\boldsymbol{x} \\
&= (c^n\,\boldsymbol{u}^{\star\star}, \nabla\mu^{n+1}).
\end{aligned} \tag{A.6}$$

Combining the discrete product derivative equality

$$\delta_t\left(a^{n+1}\,b^{n+1}\right) = \delta_t a^{n+1}\,b^n + a^{n+1}\,\delta_t b^{n+1}\,,$$

together with expressions (A.5) and (A.6), we arrive at

$$\begin{aligned}
&\gamma_{nem}\,\|\boldsymbol{w}^{n+1}\|_{L^2}^2 + \gamma_{mix}\|\nabla\mu^{n+1}\|_{L^2}^2 \\
&+ND_{philic}^{n+1} + ND_{phobic}^{n+1} + ND_{interp}^{n+1} + ND_{elast}^{n+1}(c^n) + ND_{penal}^{n+1}(c^n) + ND_{anch}^{n+1} \\
&+\lambda_{nem}\,\delta_t E_{nem}(\boldsymbol{d}^{n+1}, c^{n+1}) + \lambda_{mix}\,\delta_t E_{mix}(c^{n+1}) + \lambda_{anch}\,\delta_t E_{anch}(\boldsymbol{d}^{n+1}, c^{n+1}) \\
&= -((\boldsymbol{u}^\star\cdot\nabla)\boldsymbol{d}^n, \boldsymbol{w}^{n+1}) + (c^n\,\boldsymbol{u}^{\star\star}, \nabla\mu^{n+1}).
\end{aligned} \tag{A.7}$$

Taking $(\bar{\boldsymbol{u}}, \bar{p}) = (\boldsymbol{u}^{n+1}, p^{n+1})$ in (3.10), we obtain

$$\frac{1}{k}\left(\frac{1}{2}\|\boldsymbol{u}^{n+1}\|_{L^2}^2 - \frac{1}{2}\|\widehat{\boldsymbol{u}}\|_{L^2}^2\right) + \frac{1}{2k}\|\boldsymbol{u}^{n+1}-\widehat{\boldsymbol{u}}\|_{L^2}^2 + 2\,\|\nu(c^n)^{1/2}\boldsymbol{D}\boldsymbol{u}^{n+1}\|_{L^2}^2 = 0\,. \tag{A.8}$$

We can rewrite (3.11) as

$$\frac{\widehat{\boldsymbol{u}}-\boldsymbol{u}^\star}{2} + \frac{\widehat{\boldsymbol{u}}-\boldsymbol{u}^{\star\star}}{2} = 0\,.$$

Then, multiplying previous expression by $\frac{1}{k}\widehat{\boldsymbol{u}}$ and integrating over Ω,

$$\frac{1}{2k}\left(\|\widehat{\boldsymbol{u}}\|_{L^2}^2 - \frac{\|\boldsymbol{u}^\star\|_{L^2}^2 + \|\boldsymbol{u}^{\star\star}\|_{L^2}^2}{2} + \frac{\|\widehat{\boldsymbol{u}}-\boldsymbol{u}^\star\|_{L^2}^2 + \|\widehat{\boldsymbol{u}}-\boldsymbol{u}^{\star\star}\|_{L^2}^2}{2}\right) = 0\,. \tag{A.9}$$

We deduce multiplying (3.4) by $\dfrac{1}{k}\,\boldsymbol{u}^\star$ and (3.8) by $\dfrac{1}{k}\,\boldsymbol{u}^{\star\star}$, respectively:

$$\frac{1}{4k}\left(\|\boldsymbol{u}^\star\|_{L^2}^2 - \|\boldsymbol{u}^n\|_{L^2}^2\right) + \frac{1}{4k}\|\boldsymbol{u}^\star-\boldsymbol{u}^n\|_{L^2}^2 - ((\nabla\boldsymbol{d}^n)^t\,\boldsymbol{w}^{n+1}, \boldsymbol{u}^\star) = 0\,,$$

$$\frac{1}{4k}\left(\|\boldsymbol{u}^{\star\star}\|_{L^2}^2 - \|\boldsymbol{u}^n\|_{L^2}^2\right) + \frac{1}{4k}\|\boldsymbol{u}^{\star\star}-\boldsymbol{u}^n\|_{L^2}^2 + (c^n\nabla\mu^{n+1}, \boldsymbol{u}^{\star\star}) = 0\,.$$

DOI: 10.1002/nme

Then, adding both relations, we obtain

$$
\begin{aligned}
&-\frac{1}{2k}\,\|\boldsymbol{u}^n\|^2+\frac{1}{2k}\left(\frac{\|\boldsymbol{u}^\star\|_{L^2}^2+\|\boldsymbol{u}^{\star\star}\|_{L^2}^2}{2}\right)+\frac{1}{4k}\,\left(\|\boldsymbol{u}^\star-\boldsymbol{u}^n\|_{L^2}^2+\|\boldsymbol{u}^{\star\star}-\boldsymbol{u}^n\|_{L^2}^2\right)\\
&-\left((\nabla \boldsymbol{d}^n)^t\,\boldsymbol{w}^{n+1},\boldsymbol{u}^\star\right)+(c^n\,\nabla\mu^{n+1},\boldsymbol{u}^{\star\star})=0.
\end{aligned}
\tag{A.10}
$$

Hence, by adding expressions (A.8), (A.9), and (A.10),

$$
\begin{aligned}
&\frac{1}{2k}\left(\|\boldsymbol{u}^{n+1}\|_{L^2}^2-\|\boldsymbol{u}^n\|_{L^2}^2\right)+2\,\|\nu(c^n)^{1/2}\boldsymbol{D}\boldsymbol{u}^{n+1}\|_{L^2}^2\\
&+ND_{\boldsymbol{u}}^{n+1}-((\nabla \boldsymbol{d}^n)^t\,\boldsymbol{w}^{n+1},\boldsymbol{u}^\star)+(c^n\nabla\mu^{n+1},\boldsymbol{u}^{\star\star})=0.
\end{aligned}
\tag{A.11}
$$

Finally, adding expressions (A.7) and (A.11), we arrive at (3.13). □

Proof of Lemma 3.5
Using the Taylor expansion for $\mathcal{C}^2(\boldsymbol{R})$-functions, we obtain

$$
\begin{aligned}
\tilde{F}(c^{n+1}) &= \tilde{F}(c^n)+\tilde{F}'(c^n)\,(c^{n+1}-c^n)+\frac{1}{2}\,\tilde{F}''(\xi)\,(c^{n+1}-c^n)^2\,,\\
&= \tilde{F}(c^n)+\tilde{f}(c^n)\,(c^{n+1}-c^n)+\frac{1}{2}\,\tilde{f}'(\xi)\,(c^{n+1}-c^n)^2\,,
\end{aligned}
$$

for $\xi\in(c^n,c^{n+1})$ or $\xi\in(c^{n+1},c^n)$. In particular, it holds

$$
\delta_t\tilde{F}(c^{n+1})=\frac{1}{k}\,\tilde{f}(c^n)\,(c^{n+1}-c^n)+\frac{1}{2k}\,\tilde{f}'(\xi)\,(c^{n+1}-c^n)^2\,.
$$

On the other hand, by the definition of $f_k(c^{n+1},c^n)$ in (3.21), we have

$$
f_k(c^{n+1},c^n)\,\delta_t c^{n+1}=\frac{1}{k}\,\tilde{f}(c^n)\,(c^{n+1}-c^n)+\frac{1}{2k}\,\|\tilde{f}'\|_\infty\,(c^{n+1}-c^n)^2\,.
$$

Combining two previous expressions,

$$
\begin{aligned}
ND_{phobic}^{n+1} &= \lambda_{mix}\int_\Omega\left(f_k(c^{n+1},c^n)\delta_t c^{n+1}-\delta_t\tilde{F}(c^{n+1})\right)d\boldsymbol{x}\\
&= \lambda_{mix}\,\frac{k}{2}\int_\Omega\left(\|\tilde{f}'\|_\infty-\tilde{f}'(\xi)\right)\,|\delta_t c^{n+1}|^2 d\boldsymbol{x}\geqslant 0\,.
\end{aligned}
$$

□

Proof of Lemma 3.8
We use Lemma 4.1 from [19], where it is proven that

$$
\frac{1}{2}\,(\boldsymbol{d}^{n+1}-\boldsymbol{d}^n)^t\,H_{\boldsymbol{d}}\tilde{G}(\boldsymbol{d}^{n+\theta})\,(\boldsymbol{d}^{n+1}-\boldsymbol{d}^n)\leqslant\frac{H_{\tilde{G}}}{2}\,|\boldsymbol{d}^{n+1}-\boldsymbol{d}^n|^2,
\tag{A.12}
$$

for $H_{\tilde{G}}>0$ a bound of the L^∞-norm of the Hessian matrix $H_{\boldsymbol{d}}\tilde{G}$ associated to $\tilde{G}(\boldsymbol{d})$ (for instance, it is also proven in [19] that $H_{\tilde{G}}:=(M\,3^2+(M^2-M)\,2^2)^{1/2}$, being M the space dimension).

On one hand,

$$
\tilde{G}(\boldsymbol{d}^{n+1})=\tilde{G}(\boldsymbol{d}^n)+\tilde{\boldsymbol{g}}(\boldsymbol{d}^n)\cdot(\boldsymbol{d}^{n+1}-\boldsymbol{d}^n)+\frac{1}{2}\,(\boldsymbol{d}^{n+1}-\boldsymbol{d}^n)^t\,H_{\boldsymbol{d}}\tilde{G}(\boldsymbol{d}^{n+\theta})\,(\boldsymbol{d}^{n+1}-\boldsymbol{d}^n)\,,
$$

where $\boldsymbol{d}^{n+\theta}=\theta\,\boldsymbol{d}^n+(1-\theta)\,\boldsymbol{d}^{n+1}$, with some $\theta\in(0,1)$.

DOI: 10.1002/nme

On the other hand,

$$\boldsymbol{g}_k(\boldsymbol{d}^{n+1},\boldsymbol{d}^n)\cdot\delta_t\boldsymbol{d}^{n+1}=\frac{1}{k}\,\tilde{\boldsymbol{g}}(\boldsymbol{d}^n)\cdot(\boldsymbol{d}^{n+1}-\boldsymbol{d}^n)+\frac{1}{2k}\,H_{\tilde{\boldsymbol{G}}}\,|\boldsymbol{d}^{n+1}-\boldsymbol{d}^n|^2\,.$$

Therefore,

$$\begin{aligned}ND^{n+1}_{penal}(c)&=\lambda_{nem}\int_\Omega I(c)\,\left(\boldsymbol{g}_k(\boldsymbol{d}^{n+1},\boldsymbol{d}^n)\cdot\delta_t\boldsymbol{d}^{n+1}-\delta_t\tilde{G}(\boldsymbol{d}^{n+1})\right)d\boldsymbol{x}\\&=\frac{\lambda_{nem}}{2k}\int_\Omega I(c)\,\left((\boldsymbol{d}^{n+1}-\boldsymbol{d}^n)^t\,\left(H_{\tilde{\boldsymbol{G}}}\,\mathbb{I}-H_{\boldsymbol{d}}\tilde{\boldsymbol{G}}(\boldsymbol{d}^{n+\theta})\right)\,(\boldsymbol{d}^{n+1}-\boldsymbol{d}^n)\right)d\boldsymbol{x}\end{aligned}$$

is a positive term, thanks to (A.12). □

Proof of Lemma 3.11

Because (3.15) is an algebraic square linear system, it suffices to prove uniqueness. Indeed, let (c_1^{n+1},μ_1^{n+1}) and (c_2^{n+1},μ_2^{n+1}) be two possible solutions, and denoting $c=c_1^{n+1}-c_2^{n+1}$ and $\mu=\mu_1^{n+1}-\mu_2^{n+1}$, we arrive at

$$\left\{\begin{array}{c}(c,\bar{\mu})+2\,k^2(|c^n|^2\nabla\mu,\nabla\bar{\mu})+\gamma_{mix}\,k(\nabla\mu,\nabla\bar{\mu})=0\,,\\ \lambda_{mix}(\nabla c,\nabla\bar{c})+\dfrac{\lambda_{mix}}{\varepsilon^2}(c,\bar{c})\\ +\lambda_{nem}\dfrac{5\sqrt{3}}{12}\left(\left(\dfrac{1}{2}|\nabla\boldsymbol{d}^n|^2+G(\boldsymbol{d}^n)\right)c,\bar{c}\right)\\ +\lambda_{anch}(\Lambda_c(\boldsymbol{d}^n,c),\nabla\bar{c})-(\mu,\bar{c})=0\,,\end{array}\right.\tag{A.13}$$

where $\left(\frac{1}{2}|\nabla\boldsymbol{d}^n|^2+G(\boldsymbol{d}^n)\right)\geqslant 0$ and $\Lambda_c(\boldsymbol{d}^n,c)$ was defined in (3.9). Then, taking $(\bar{\mu},\bar{c})=(\mu,c)$, we obtain

$$\begin{aligned}&2\,k^2\int_\Omega|c^n|^2|\nabla\mu|^2d\boldsymbol{x}+\gamma_{mix}\,k\|\nabla\mu\|_{L^2}^2+\lambda_{mix}\|\nabla c\|_{L^2}^2+\frac{\lambda_{mix}}{\varepsilon^2}\|c\|_{L^2}^2\\&\qquad+\lambda_{nem}\frac{5\sqrt{3}}{12}\int_\Omega\left(\frac{1}{2}|\nabla\boldsymbol{d}^n|^2+G(\boldsymbol{d}^n)\right)|c|^2d\boldsymbol{x}+\lambda_{anch}\Phi(\boldsymbol{d}^n,c)=0\,,\end{aligned}$$

with

$$\Phi(\boldsymbol{d},c)=\int_\Omega\left(\delta_1\,|\boldsymbol{d}|^2\,|\nabla c|^2+\delta_2\,|\boldsymbol{d}\cdot\nabla c|^2\right)d\boldsymbol{x}\geqslant 0\,.\tag{A.14}$$

Because $\dfrac{1}{2}|\nabla\boldsymbol{d}^n|^2+G(\boldsymbol{d}^n)\geqslant 0$, then $\nabla\mu=\nabla c=0$ and $c=0$ in Ω. In particular, $\mu=C=const$. By returning to $(A.13)_2$, we have

$$(\mu,\bar{c})=C\,(1,\bar{c})=0\quad\forall\,\bar{c}\in C_h.$$

Therefore, if $1\in C_h$, then $C=0$. □

Proof of Lemma 3.12

Because (3.16) is an algebraic square linear system, it suffices to prove uniqueness. Indeed, let $\left(\boldsymbol{d}_1^{n+1},\boldsymbol{w}_1^{n+1}\right)$ and $\left(\boldsymbol{d}_2^{n+1},\boldsymbol{w}_2^{n+1}\right)$ be two possible solutions, and denoting $\boldsymbol{d}=\boldsymbol{d}_1^{n+1}-\boldsymbol{d}_2^{n+1}$ and $\boldsymbol{w}=\boldsymbol{w}_1^{n+1}-\boldsymbol{w}_2^{n+1}$, we arrive at

DOI: 10.1002/nme

$$\begin{cases} (\boldsymbol{d},\bar{\boldsymbol{w}}) + 2\,k^2((\nabla \boldsymbol{d}^n)^t\,\boldsymbol{w},(\nabla \boldsymbol{d}^n)^t\,\bar{\boldsymbol{w}}) + \gamma_{nem}\,k(\boldsymbol{w},\bar{\boldsymbol{w}}) = 0\,, \\ \lambda_{nem}(I(c^{n+1})\nabla \boldsymbol{d},\nabla \bar{\boldsymbol{d}}) + \dfrac{\lambda_{nem}}{2}\|\widetilde{\boldsymbol{g}}'\|_\infty(I(c^{n+1})\boldsymbol{d},\bar{\boldsymbol{d}}) \\ \qquad\qquad +\lambda_{anch}(\Lambda_{\boldsymbol{d}}(\boldsymbol{d},c^{n+1}),\bar{\boldsymbol{d}}) - (\boldsymbol{w},\bar{\boldsymbol{d}}) = 0, \end{cases} \tag{A.15}$$

where we remind that $I(c^{n+1}) \geqslant 0$ and $\Lambda_{\boldsymbol{d}}(\boldsymbol{d},c^{n+1})$ was defined in (3.5). Then, taking $(\bar{\boldsymbol{w}},\bar{\boldsymbol{d}}) = (\boldsymbol{w},\boldsymbol{d})$, we obtain

$$\begin{aligned} &2\,k^2\|\nabla \boldsymbol{d}^n\boldsymbol{w}\|^2 + \gamma_{nem}\,k\|\boldsymbol{w}\|_{L^2}^2 + \lambda_{nem}\int_\Omega I(c^{n+1})|\nabla \boldsymbol{d}|^2 d\boldsymbol{x} \\ &+\frac{\lambda_{nem}}{2}\|\widetilde{\boldsymbol{g}}'\|_\infty\int_\Omega I(c^{n+1})|\boldsymbol{d}|^2 d\boldsymbol{x} + \lambda_{anch}\Phi(\boldsymbol{d},c^{n+1}) = 0 \end{aligned}$$

for Φ defined in (A.14). From the previous relation, we obtain $\boldsymbol{w} = 0$ in Ω. Then using this information in $(A.15)_1$, we deduce

$$(\boldsymbol{d},\bar{\boldsymbol{w}}) = 0 \qquad \forall\,\bar{\boldsymbol{w}} \in \boldsymbol{W}_h;$$

hence, $\boldsymbol{d} = 0$ in Ω if we assume $\boldsymbol{D}_h \subseteq \boldsymbol{W}_h$. □

Proof of Lemma 3.13

Because (3.17) is an algebraic square linear system, it suffices to prove uniqueness. Indeed, let $(\boldsymbol{u}_1^{n+1},p_1^{n+1})$ and $(\boldsymbol{u}_2^{n+1},p_2^{n+1})$ be two possible solutions, and denoting $\boldsymbol{u} = \boldsymbol{u}_1^{n+1} - \boldsymbol{u}_2^{n+1}$ and $p = p_1^{n+1} - p_2^{n+1}$, we arrive at

$$\begin{cases} \dfrac{1}{k}(\boldsymbol{u},\bar{\boldsymbol{u}}) + c(\boldsymbol{u}^n,\boldsymbol{u},\bar{\boldsymbol{u}}) - (p,\nabla\cdot\bar{\boldsymbol{u}}) + 2\,(\nu(c^{n+1})\boldsymbol{D}\boldsymbol{u},\boldsymbol{D}\bar{\boldsymbol{u}}) = 0\,, \\ (\nabla\cdot\boldsymbol{u},\bar{p}) = 0\,. \end{cases} \tag{A.16}$$

Testing by $(\bar{\boldsymbol{u}},\bar{p}) = (\boldsymbol{u},p)$, we obtain

$$\frac{1}{k}\|\boldsymbol{u}\|_{L^2}^2 + 2\int_\Omega \nu(c^{n+1})|\boldsymbol{D}\boldsymbol{u}|^2 = 0 \quad \Rightarrow \quad \boldsymbol{u} = 0\,.$$

Using this information we obtain from $(A.16)_1$,

$$(p,\nabla\cdot\bar{\boldsymbol{u}}) = 0 \quad \forall\,\bar{\boldsymbol{u}} \in \boldsymbol{V}_h.$$

Therefore, assuming that the pair of finite element spaces $(\boldsymbol{V}_h,P_h)$ satisfies the discrete *inf-sup* condition (3.29), we can infer $p = 0$ in Ω. □

ACKNOWLEDGEMENTS

This research has been partially supported by MINECO grant MTM2012-32325 (Ministerio de Economía y Competitividad, Spain) with the participation of FEDER. Giordano Tierra has also been partially supported by ERC-CZ project LL1202 (Ministry of Education, Youth and Sports of the Czech Republic).The authors would like to thank the referees for their valuable comments, which helped to improve the manuscript.

REFERENCES

1. van der Waals JD. The thermodynamic theory of capillarity flow under the hypothesis of a continuous variation of density. *Journal of Statistical Physics* 1979; **20**:197–244.
2. Collings PJ. *Liquid Crystals: Nature's Delicate Phase of Matter*. Princeton University Press: Princeton, New Jersey, 1990.
3. Tierra G, Guillén-González F. Numerical methods for solving the Cahn–Hilliard equation and its applicability to related energy–based models. *Archives of Computational Methods in Engineering* 2015; **22**:269–289.
4. Kim J. Phase-field models for multi-component fluid flows. *Communications in Computational Physics* 2012; **196**:613–661.

DOI: 10.1002/nme

5. Badia S, Guillén-González F, Gutiérrez-Santacreu JV. An overview on numerical analyses of nematic liquid crystal flows. *Archives of Computational Methods in Engineering* 2011; **18**:285–313.
6. Climent-Ezquerra B, Guillén-González F. A review of mathematical analysis of nematic and smectic-A liquid crystal models. *European Journal of Applied Mathematics* 2013; **10**:1–21.
7. Denniston C, Orlandini E, Yeomans JM, Phase ordering in nematic liquid crystals, Physical Review E, 2001; **64**:021701.
8. Andrienko D, Tasinkevych M, Patricio P, Telo da Gama MM. Interaction of colloids with a nematic–isotropic interface. *Physical Review E* 2004; **69**:021706.
9. van Bijnen RMW, Otten RHJ, van der Schoot P. Texture and shape of two-dimensional domains of nematic liquid crystals. *Physical Review E* 2012; **86**:051703.
10. Kim YK, Shiyanovskii SV, Lavrentovich OD. Morphogenesis of defects and tactoids during isotropic–nematic phase transition in self-assembled lyotropic chromonic liquid crystals. *Journal of Physics: Condensed Matter* 2013; **25**:404202.
11. Bernardino NR, Figueirinhas Pereira MC, Silvestre NM, Telo da Gama MM. Structure of the cholesteric–isotropic interface. *Soft Matter* 2014; **64**:9399.
12. Yue P, Feng JJ, Liu C, Shen J. A diffuse-interface method for simulating two-phase flows of complex fluids. *Journal of Fluid Mechanics* 2004; **515**:293–317.
13. Feng JJ, Liu C, Shen J, Yue P. An energetic variational formulation with phase field methods for interfacial dynamics of complex fluids: advantages and challenges. In *Modeling of Soft Matter*. Springer: New York, 2005; 1–26.
14. Yue P, Feng JJ, Liu C, Shen J. Interfacial forces and Marangoni flow on a nematic drop retracting in an isotropic fluid. *Journal of Colloid and Interface Science* 2005; **290**:281–288.
15. Yang X, Forest MG, Li H, Liu C, Shen J, Wang Q, Chen F. Modeling and simulations of drop pinch-off from liquid crystal filaments and the leaky liquid crystal faucet immersed in viscous fluids. *Journal of Computational Physics* 2013; **236**:1–14.
16. Shen J, Yang X. Decoupled energy stable schemes for phase field models of two-phase complex fluids. *SIAM Journal of Scientific Computing* 2014; **36**:122–145.
17. Minjeaud S. An unconditionally stable uncoupled scheme for a triphasic Cahn–Hilliard/Navier–Stokes model. *Numerical Methods for Partial Differential Equations* 2013; **29**:584–618.
18. Guillén-González F, Tierra G. Splitting schemes for a Navier–Stokes–Cahn–Hilliard problem modeling two-fluids with different densities. *Journal of Computational Mathematics* 2014; **32**:643–664.
19. Cabrales RC, Guillén-González F, Gutiérrez-Santacreu JV. A time-splitting finite-element stable approximation for the Ericksen–Leslie equations. *SIAM Journal of Scientific Computing* 2015; **37**:261–282.
20. Cahn JW, Hilliard JE. Free energy of a nonuniform system. I. Interfacial free energy. *Journal of Chemical Physics* 1958; **28**:258–267.
21. Boyer F, Chupin L, Fabrie P. Numerical study of viscoelastic mixtures through a Cahn–Hilliard flow model. *European Journal of Mechanics B/Fluids* 2004; **23**:759–780.
22. Liu C, Shen J. A phase field model for the mixture of two incompressible fluids and its approximation by a Fourier-spectral method. *Physica D* 2003; **179**:211–228.
23. Yang X, Feng JJ, Liu C, Shen J. Numerical simulations of jet pinching-off and drop formation using an energetic variational phase-field method. *Journal of Computational Physics* 2006; **218**:417–428.
24. Du Q, Liu C, Ryham R, Wang X. Energetic variational approaches to modeling vesicle and fluid interactions. *Physica D* 2009; **238**:923–930.
25. Tierra G, Pavissich JP, Nerenberg R, Xu Z, Alber MS. Multicomponent model of deformation and detachment of a biofilm under fluid flow. *Journal of The Royal Society Interface* 2015; **12**:20150045.
26. Hyon Y, Eisenberg R, Liu C. An energetic variational approach to ion channel dynamics. *Mathematical Methods in the Applied Sciences* 2011; **37**:952–961.
27. Hyon Y, Kwak Y, Liu C. Energetic variational approach in complex fluids: maximum dissipation principle. *Discrete and Continuous Dynamical Systems - Series A* 2010; **26**:1291–1304.
28. Sun H, Liu C. On energetic variational approaches in modeling the nematic liquid crystal flows. *Discrete and Continuous Dynamical Systems* 2009; **23**:455–475.
29. Elliott CM, Garcke H. On the Cahn–Hilliard equation with degenerate mobility. *SIAM Journal on Mathematical Analysis. SIAM* 1996; **27**(2):404–423.
30. Guillén-González F, Tierra G. On linear schemes for a Cahn–Hilliard diffuse interface model. *Journal of Computational Physics* 2013; **234**:140–171.
31. Guillén-González F, Tierra G. Second order schemes and time-step adaptivity for Allen–Cahn and Cahn–Hilliard models. *Computers & Mathematics with Applications* 2014; **68**:821–846.
32. Eyre DJ. An unconditionally stable one-step scheme for gradient system. Available from: http://www.math.utah.edu/eyre/research/methods/stable.ps, unpublished. [accessed date May 26, 1998].
33. Shen J, Yang X. Numerical approximations of Allen–Cahn and Cahn–Hilliard equations. *Discrete and Continuous Dynamical Systems* 2010; **28**:1669–1691.
34. Hecht F. New development in FreeFem++. *Journal of Numerical Mathematics* 2012; **20**:251–265.

DOI: 10.1002/nme